Effects of Manufacturing Deviations on Core Compressor Blade Performance

Clayton Ray De Losier

Thesis submitted to the faculty of the Virginia Polytechnic Institute and State University in partial fulfillment of the requirements for the degree of

Master of Science
in
Mechanical Engineering

Wing Ng, Ph.D.
Walter O'Brien, Ph. D.
Srinath Ekkad, Ph. D.

02/20/09
Blacksburg, VA

Keywords: principal component analysis, gas turbine compressor, manufacturing deviations, leading edge, MISES

Effects of Manufacturing Deviations on Core Compressor Blade Performance

Clayton Ray De Losier

ABSTRACT

There has been recent incentive for understanding the possible deleterious effects that manufacturing deviations can have on compressor blade performance. This is of particular importance in today's age, as compressor designs are pushing operating limits by employing fewer stages with higher loadings and are designed to operate at ever higher altitudes. Deviations in these advanced, as well as legacy designs, could negatively affect the performance and operation of a core compressor; thus, a numerical investigation to quantify manufacturing deviations and their effects is undertaken. Data from three radial sections of every compressor blade in a single row of a production compressor is used as the basis for this investigation. Deviations from the compressor blade design intent to the as-manufactured blades are quantified with a statistical method known as principle component analysis (PCA). MISES, an Euler solver coupled with integral boundary-layer calculations, is used to analyze the effects that the aforementioned deviations have on compressor blade performance when the inlet flow conditions produce a Mach number of approximately 0.7 and a Reynolds number of approximately 6.5×10^5. It was found that the majority of manufacturing deviations were within a range of plus or minus 4% of the design intent, and deviations at the leading edge had a critical effect on performance. Of particular interest is the fact that deviations at the leading edge not only degraded performance but significantly changed the boundary-layer behavior from that of the design case.

ACKNOWLEDGEMENTS

TABLE OF CONTENTS

LIST OF FIGURES

LIST OF TABLES

NOMENCLATURE

C	covariance matrix of the data matrix for principal component analysis
C_f	skin-friction coefficient
DATA	a column containing a set of x-y coordinate differences between the design intent and the as-manufactured compressor blade shapes, where the mean of the differences between the design intent and the as-manufactured compressor blade shapes, for every set of x-y coordinates, is removed
DESG	a set of x-y coordinates that define the compressor blade shape for the intended design
ER	a set of x-y coordinate differences between the design intent and the as-manufactured compressor blade shapes
H	boundary-layer shape parameter
L.E.	leading edge
m'	non-dimensional axial distance
MEAN	a column containing the mean of the differences between the design intent and the as-manufactured compressor blade shapes for every set of x-y coordinates
MFG	a set of x-y coordinates for each as-manufactured compressor blade shape
MODE	a column containing the information necessary to reconstruct the principal components in terms of two-dimensional compressor blade shapes
n	total number of compressor blades
NBLPKZ	number of points axially clustered
NBLPTT	number of points in the theta direction
NBLPTZ	number of points on the blade surface in the axial direction
p	total number of x-y coordinate points that define a compressor blade shape
T.E.	trailing edge
U	a matrix containing the eigenvectors that correspond to the eigenvalues of the covariance matrix, where the covariance matrix is based on the transpose of the data matrix used for singular value decomposition
V	a matrix containing the eigenvectors that correspond to the eigenvalues of the covariance matrix, obtained via singular value decomposition
X	a data matrix in mean-deviation form, for principal component analysis
x	a matrix containing the eigenvectors that correspond to the eigenvalues of the covariance matrix, obtained via principal component analysis
Y	a data matrix in mean-deviation form, for singular value decomposition

Greek

λ a matrix containing the eigenvalues of the covariance matrix, obtained via principal component analysis

Σ a matrix containing the eigenvalues of the covariance matrix, obtained via singular value decomposition

θ inlet flow angle

Superscripts

T   transpose

1. INTRODUCTION

This thesis is based on the desire to not only quantify the manufacturing deviations of the compressor blades present in an individual rotor of an operational core compressor, but to also quantify the effects that those manufacturing deviations have on the compressor blade's performance. The following sections of this chapter are thus used to describe the motivations for investigating the aforementioned research topics and the research objectives needed to shape those research topics into tangible results.

1.1 Motivation

The motivation for the current investigation stems from the need to understand the effects that manufacturing deviations have on compressor blade performance, which is of particular interest considering the incentives for developing more highly loaded machines. A review of the current literature offers some insight into the quantification of manufacturing deviations in as-manufactured compressor blades and the possible deleterious effects that manufacturing deviations can have on individual compressor blade performance, however, the focus tends to mainly be on robust design methods.

Investigations into producing more robust compressor blade designs, based on manufacturing deviations in as-manufactured compressor blades, has mainly been carried out by two sets of authors, Lamb and Darmofal [1] and Garzon and Darmofal [2]. To carry out their work, both sets of authors employed principal component analysis to quantify manufacturing deviations and various types of numerical simulations to gain information for the improvement of robust design methods; the most crucial numerical simulation being a Monte Carlo simulation. This implementation of Monte Carlo simulations, in conjunction with different types of assumed statistical distributions, allowed both sets of authors to use larger sample sizes in their Monte Carlo simulations and identify the areas of compressor blade design that required more attention than others when accounting for manufacturing effects in compressor blade performance.

Similar work for the improvement of robust gas turbine blade design methods, via the incorporation of manufacturing deviation effects, has also been found in the literature. One typical example is the research done by Burton et al. [3]. In this study an investigation on the improvement of two different reliability design methods for gas turbine blades, through the use of finite element analysis (FEA), is undertaken, where the creation of the variations in the investigated turbine blade geometries is carried out through the use of two shape parameters that are generated from two assumed Gaussian random variables. Some other works in the area of robust gas turbine blade design, such as those by Sidwell and Darmofal [4] and Moeckel et al. [5], also improve upon the design methodology for gas turbine blades, but model the variability in their probabilistic analyses with known geometrical variations from as-manufactured parts.

Despite this use of known geometrical variations, instead of assumed distributions, these works and all of the other aforementioned works only elucidate improved design methods in light of manufacturing deviations. None of the reviewed works reveal specifically how manufacturing deviations alter compressor blade performance. Therefore, to help broaden the scope of research that has already been carried out, this work implements principal component analysis to quantify the departures

in as-manufactured compressor blades from their design intent for a single rotor and undertakes a detailed investigation of the effects that those manufacturing deviations have on the compressor blade's performance; noting that the methods presented, particularly the implementation of principal component analysis and the extension of those results to other, yet to be manufactured, compressor blades, is more applicable than the investigation of a specific compressor rotor.

1.2 Research Objectives

There is one minor and two major research objectives covered by this thesis. The first major research objective is to implement a statistical method known as principal component analysis to quantify the manufacturing deviations present at three different radial sections of a single bladerow in a production compressor. Concurrent with the first major objective, the second major objective is to use the boundary layer-inviscid coupled solver MISES to identify the performance effects that the greatest manufacturing deviations have at each of the three radial locations. And finally, the only minor research objective that this thesis covers is a method for applying principal component analysis results from one blade shape to another.

1.3 Thesis Structure

The structure of this thesis is laid out in a four chapter format with accompanying appendices. Chapter 1 covers the motivation behind the research that was carried out, while Chapter 2 covers the mathematical details of principal component analysis and the results obtained from the principal component analysis of the three aforementioned radial sections. Chapter 3 covers the details of the numerical methods used to investigate the aerodynamic effects from the greatest manufacturing deviations at each of the three radial locations; corresponding results from that numerical analysis are also presented. Overarching conclusions drawn from the results presented in Chapters 2 and 3 are then presented in Chapter 4, where recommendations for future work and a discussion on the method for applying principal component analysis results from one blade shape to another are also provided. Finally, the appendices cover supplemental numerical and principal component analysis information.

2. PRINCIPAL COMPONENT ANALYSIS

This chapter covers the basic theory and mathematics of principal component analysis, where emphasis is placed on applications to radial cross sections of gas turbine compressor blades. Results from the application of principal component analysis to an individual rotor of an operational core compressor is then presented, where the data used in the analysis is coordinate measuring machine data taken from a fabricated engine.

Further elucidation of the mathematics behind principal component analysis and the principal component analysis code developed at Virginia Tech, to specifically handle two-dimensional compressor blade data, can be found in Appendix A.

2.1 Principal Component Analysis Overview

Principal component analysis is a common multivariate statistical technique and has been around since the early twentieth century [6]. Several books have been written on the matter and describe, in general mathematical terms, the theory and mathematics behind principal component analysis [6-9]. Therefore, this section avoids reiterating material that is readily available and focuses on principal component analysis in more specific terms, where particular attention is placed on explaining how principal component analysis is applied to two-dimensional compressor blade data.

The first task in applying principal component analysis to two-dimensional compressor blade data is to calculate the x-y coordinate differences between the design intent and the as-manufactured blades, referred to as the error vectors, for all of the measured as-manufactured blades used in the analysis. Once the error vectors for all of the as-manufactured blades have been calculated they are combined into a single data matrix, as shown in Figure 2.1, where the data matrix now represents all of the deviations created in the process of manufacturing a set of compressor blades.
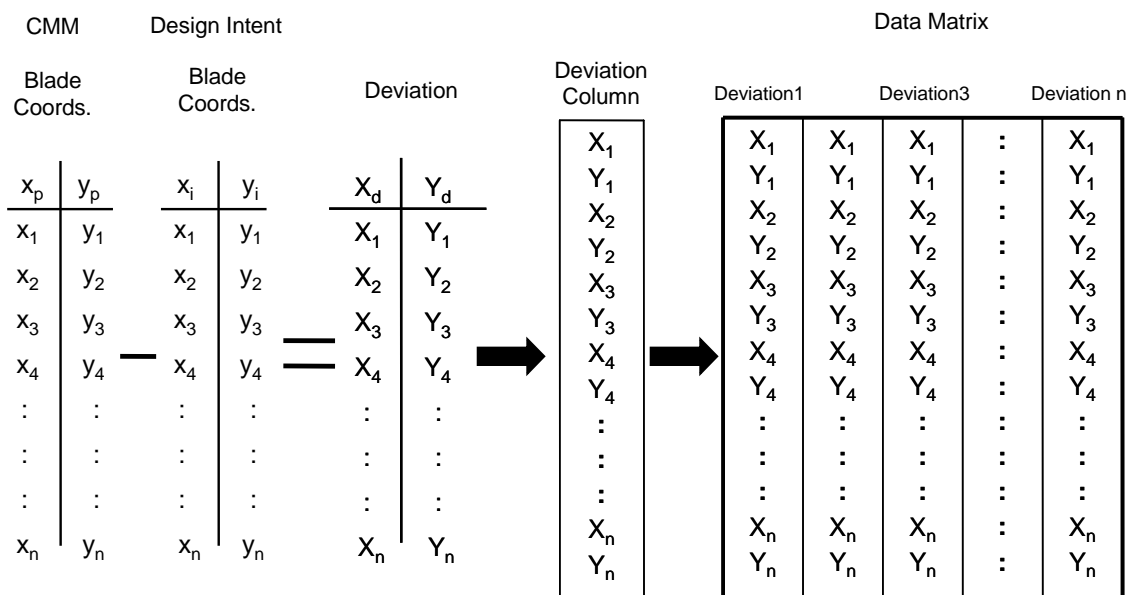
Figure 2.1. Visual representation on how to obtain a data matrix

The data matrix is then utilized to create a covariance matrix. Creation of the covariance matrix allows for the variance and covariance in the as-manufactured blade data to be described and facilitates the implementation of the remaining principal component analysis process. In the final steps of applying principal component analysis to two-dimensional compressor blade data the calculation of the principal components and the determination of the mode vectors is carried out, where the mode vectors use the principal components to represent the deviations between the as-manufactured blades and the design intent as actual two-dimensional compressor blade shapes in x-y space.

In order to make the most efficient use of the mode vectors, they are order from those that represent the greatest amount of deviation between the design intent and the as-manufactured blades to those that contain the least amount of variation. Thus, the first mode vector is a two-dimensional compressor blade shape that represents the greatest amount of deviation from the as-manufactured blades to the design intent and is considered the worst case scenario.

2.2 Principal Component Analysis Results

Principal component analysis was employed to quantify the greatest amount of manufacturing deviation present in one rotor of an operational core compressor. Measurements at three radial sections: hub, mid-span, and tip, for each blade in the bladerow, constituted the three disparate data sets employed with the principal component analysis, where all of the two-dimensional blade profiles in each data set were obtained via a coordinate measuring machine. The results from the principal component analysis were analyzed by inspecting the amount of deviation contained in each mode and then using the common geometric parameters from similar studies [1-2] to quantify the differences between mode 1 and the design intent; noting that, by definition of Eq. A1.6 in Appendix A, mode 1 always represents the greatest amount of deviation.

2.2.1 Hub Section

The results from the principal component analysis for the hub section of the bladerow revealed that 62% of the deviation in the as-manufactured blades is represented by mode 1, and that the first six modes represent 99% of the total deviation, Figure 2.2. A quantification of the deviation represented by mode 1, Table 2.1, reveals that there is a decrease in the leading and trailing-edge thicknesses from the design intent, while there are no significant deviations to chord length or mid-chord thickness. Visualization of the deviations at the leading and trailing edges, via Figure 2.3, confirms that the deviations represented by mode 1 produce thinner leading and trailing edges, but also reveals information about the differences between the mode 1 and design intent edge profiles. The profile of the leading edge, albeit smaller than the design intent, does not have a noticeably altered leading-edge profile; however, the decrease in trailing-edge thickness is accompanied by a markedly increased roundness of the trailing-edge profile. Overall, it can then be stated, that the majority of deviation at the hub section of the bladerow is manifested as thinner leading and trailing-edge thicknesses, accompanied by a significant rounding of the trailing edge.
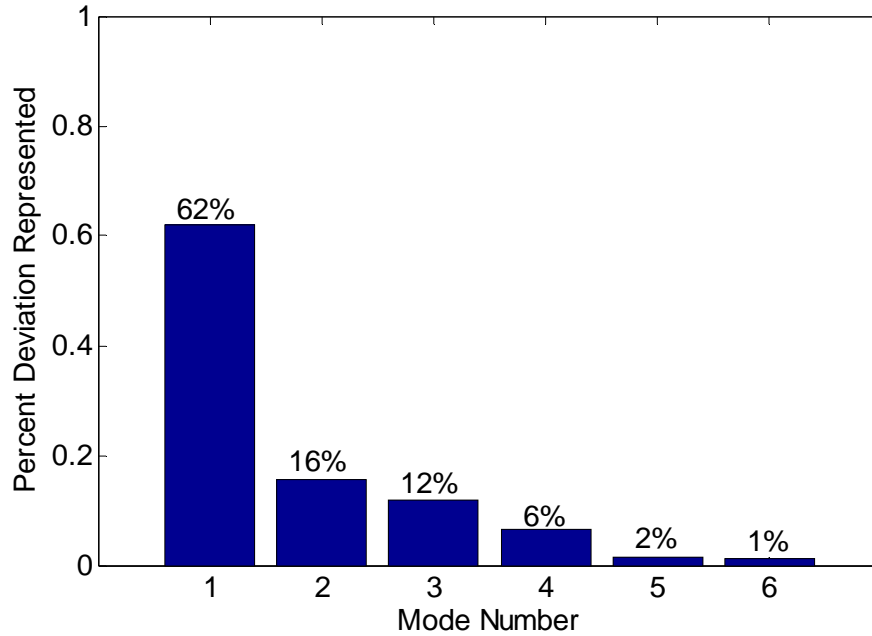
Figure 2.2. Percent deviation represented by the first six modes of the hub section
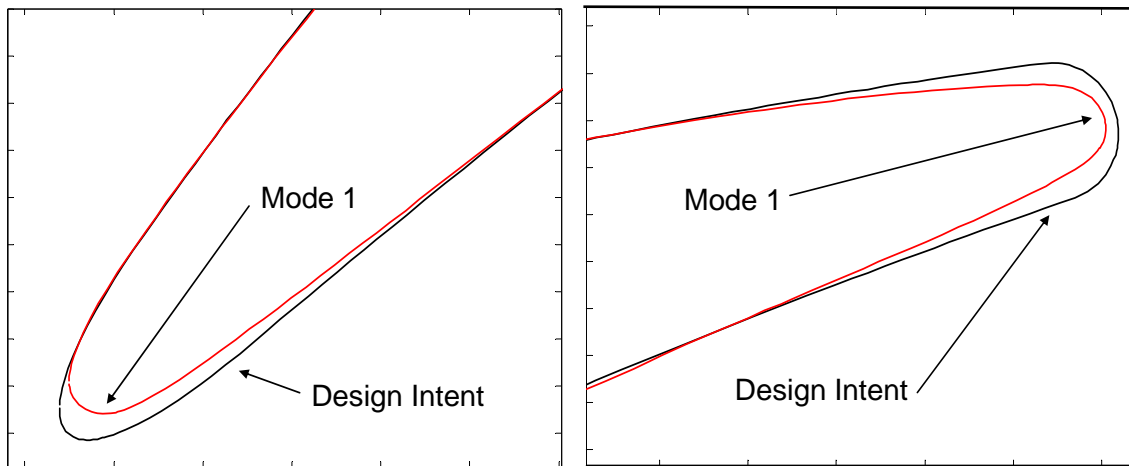
Figure 2.3. Hub section mode 1 and design intent leading and trailing-edge profiles

2.2.2 Mid-Span Section

The results from the principal component analysis for the mid-span section of the bladerow revealed that 55% of the deviation in the as-manufactured blades is represented by mode 1, with mode 2 accounting for another 21% and mode 3 accounting for 16%. And similar to the results from the hub section, the first six modes represent 99% of the total deviation from the design intent. A quantification of the deviation represented by mode 1, Table 2.1, reveals that there is a decrease in the mid-chord and trailing-edge thicknesses from the design intent, while there is an increase in leading-edge thickness. Visualization of the deviations at the leading and trailing edges, via Figure 2.4, confirms

5

that the deviations represented by mode 1 produce a thinner trailing edge and a thicker leading edge. Figure 2.4 also reveals information about the differences between the mode 1 and design intent edge profiles. The profile of the leading edge, albeit larger than the design intent, shows only a slight blunting of the leading-edge profile; however, the decrease in trailing-edge thickness is accompanied by a noticeable increase in the pressure side slope leading into the trailing-edge profile, which exhibits a slight increase in roundness over that of the design intent. Overall, it can then be stated, that the majority of deviation at the mid-span section of the blade row is manifested as a thicker leading edge and thinner mid-chord and trailing-edge thicknesses, which are accompanied by an increase in the pressure side slope leading into the trailing-edge profile.
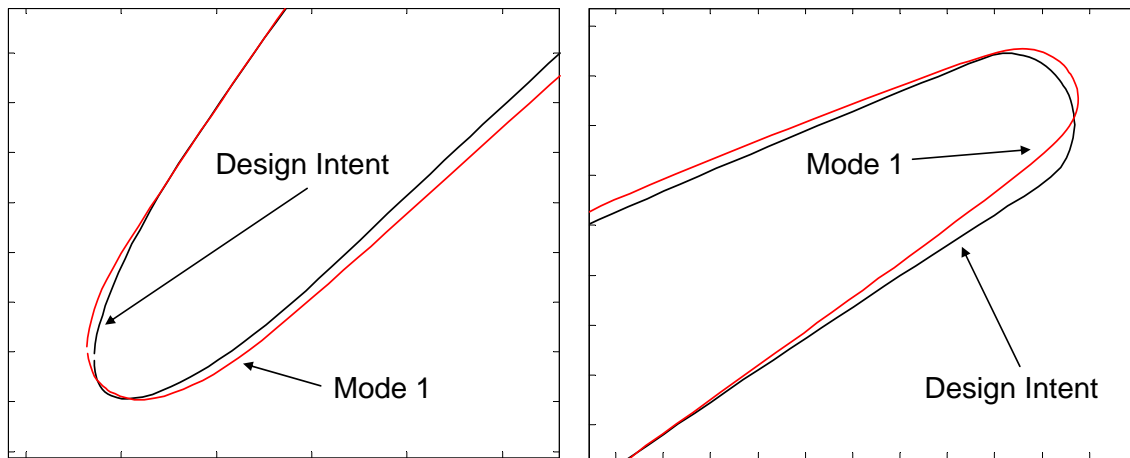
Figure 2.4. Mid-Span mode 1 and design intent leading and trailing-edge profiles

2.2.3 Tip Section

The results from the principal component analysis for the tip section of the bladerow revealed that 74% of the deviation in the as-manufactured blades is represented by mode 1, with mode 2 accounting for another 13% and mode 3 accounting for 8%. And similar to the results from the previous two sections, the first six modes represent 99% of the total deviation from the design intent. A quantification of the deviation represented by mode 1, Table 2.1, reveals that there is a significant increase in the mid-chord thickness from the design intent, while there are negligible increases in leading and trailing-edge thicknesses. Visualization of the deviations along the chord length of the blade confirms that the deviations represented by mode 1 produce a substantial increase in mid-chord thickness and slightly thicker trailing and leading edges. The visual inspection of the blade profile also reveals that the differences between the mode 1 and design intent leading-edge profiles are almost indistinguishable; however, the minute increase in trailing-edge thickness is accompanied by a moderate rounding of the trailing-edge profile. Overall, it can then be stated, that the majority of deviation at the tip section of the bladerow is manifested as a thicker mid-chord thickness and a moderate rounding of the trailing-edge profile.

	Percent Deviations from Design Intent			
Radial Section	Chord Length	L.E. Thickness (At 5% Chord)	Mid-Chord Thickness (At 50% Chord)	T.E. Thickness (At 95% Chord)
Hub	-0.6	-3.8	0.1	-4.6
Mid-Span	0.9	3.9	-3.6	-3.7
Tip	0.3	1.2	6.2	0.4

Table 2.1. Mode 1 percent deviations from design intent at each radial section

2.3 Principal Component Analysis Conclusions

In conclusion, there were several consistent trends in the results of the principal component analysis for the three radial sections investigated. At each radial section, the first six modes were able to represent 99% of the total deviation between the as-manufactured blade data sets and the design intent, were as previously explained, mode 1 always represented the greatest amount deviation. With that reiterated, the majority of deviations between the design intent and mode 1 for each radial section were within plus or minus 4%, with deviations in chord length at each of the radial sections being minute. The trailing-edge profiles for mode 1 at all three radial locations exhibited an increase in rounding over that of the design intent trailing-edge profile, and only the leading-edge profile of mode 1 at the mid-span radial location manifested a notable change, in which there was a blunting of the leading-edge profile over that of the design intent. However, despite so many similar trends occurring throughout the principal component analysis results for each radial location, the most important conclusion that can be drawn is the fact that the greater the amount of deviation represented by mode 1 the less deviation there is throughout the as-manufactured blade data set from the design intent, thus, indicating a concentration of the manufacturing deviations to a couple or even a single geometric parameter.

3. NUMERICAL ANALYSIS

Chapter 3 covers the numerical analysis employed to quantify the performance effects that the greatest manufacturing deviations identified in the previous chapter, referred to as mode 1, have on each of the three radial sections previously investigated. As support for the numerical analysis technique employed, an overview of why MISES was chosen to carry out the numerical simulations is first presented, where Appendix B provides verification of the numerical analysis employed by presenting an outline of a grid independent study. An outline of how the numerical analysis was carried out is then provided. And finally, the chapter is concluded with the results from the numerical analysis of mode 1 at each of the three radial sections investigated, where it should be noted, that reference to specific design values is omitted or rephrased in consideration of Rolls Royce's proprietary concerns.

3.1 Factors in MISES' Implementation

MISES' ability to produce quick convergence times and its sensitivity to small geometric variations, particularly near the leading edge, were the two driving factors for using MISES to carry out the numerical simulations in this study. Other codes, such as ADPAC, were initially intended to be employed for the numerical simulations in this study, as outlined in Appendix C, but ADPAC's convergence times and sheared H-mesh sensitivity levels to small geometric variations were not as desirable in comparison to MISES.

Convergence times for MISES were significantly faster than ADPAC, as MISES provided enough converged solutions to create an adequate loss bucket for one compressor blade geometry in approximately the same amount of time that it took ADPAC to converge on a solution for a single flow angle. The faster convergence times were mainly attributed to the fact that MISES is an inviscid-viscous solver that models boundary-layer transition with a modified Abu-Ghannam/Shaw (ABS) criterion coupled with e^n correlations. Coupling of the ABS criterion and the e^n correlations are handled with a modified Mack correlation, where the point at which transition occurs is based on correlations between boundary-layer shape parameter and momentum-thickness Reynolds number [19]. MISES' modeling of the inviscid flow field is handled by projecting the three-dimensional Euler equations onto an axi-symmetric flow surface of varying thickness and radius and modeling of the viscous boundary layer is handled with a two-dimensional integral boundary-layer formation; the coupling of the inviscid-viscous regions being done via the displacement thickness [12-13]. All of this is in contrast to ADPAC's use of a more complicated finite-volume based code to model the flow field via a numerical solution to the three-dimensional Reynolds-Averaged Navier-Stokes (RANS) equations [14].

ADPAC's use of the RANS equations also imposed more exacting mesh requirements for modeling the boundary-layer region, which is where the majority of losses caused by small geometric variations are manifested. A grid independent sheared H-mesh for ADPAC was used in the initial studies, however, the results from using the independent sheared H-grid, as seen in Appendix C, were still inadequate in properly resolving the boundary layer when compared to MISES' results. A better grid for

capturing the boundary layer effects caused by small geometric variations could have possibly been obtained with more intense grid generating efforts, such as the use of an appropriate O-mesh, but this would have only added to the total effort required to obtain a converged solution with ADPAC. Thus, MISES' use of a two-dimensional integral boundary-layer formation to model the boundary layer and its built in mesh generator allowed for the ability to quickly generate meshes and model the boundary layer with the resolution necessary to pick up on the subtle differences that small geometric variations impart on boundary-layer behavior.

3.2 Numerical Analysis and Results

As previously mentioned, MISES is employed to carry out a numerical analysis on how the mode 1 compressor blade shapes, as identified by principal component analysis, alter aerodynamic performance from that of the design intent. To model the two-dimensional flow for the compressor blades representing mode 1 and the design intent at the three different radial locations, a specific set of solution constraints and variables were employed. A leading and trailing edge Kutta condition and inlet slope were used as the solution constraints and exit flow slope, inlet flow slope, and leading edge stagnation point were used as the solution variables. Implementation of these solution constraints and variables were inline with the MISES' [15] recommendations on how to model fixed mass-flow rate, subsonic flow conditions, where flow conditions at the inlet to each of the radial sections of the investigated rotor are a Mach number of approximately 0.7 and a Reynolds number of approximately 6.5 x 10^5.

The implementation of MISES with the aforementioned constraints and variables, in conjunction with the operating parameters for the investigated rotor, facilitated the creation of mixed-out loss buckets for the compressor blades that represented mode 1 and the design intent at each of the three radial sections investigated. Inspection of the differences between the mixed-out loss buckets for mode 1 and the design intent were employed to determine the changes in aerodynamic performance caused by the greatest manufacturing deviations, where the mixed-out loss coefficient is defined as the ratio of the difference between the isentropic outlet stagnation pressure and the actual outlet stagnation pressure to the difference between the inlet stagnation pressure and the inlet static pressure [15].

The only addition to the use of the mixed-out loss buckets as the sole identifier of alterations to aerodynamic performance occurred at the mid-span section, as the differences between the mixed-out loss buckets for this section, from inlet flow angles of alpha one to alpha two, displayed the most significant changes in performance for the three radial sections investigated. Thus, to gain a more detailed understanding on the effects that the greatest manufacturing deviations have on compressor blade aerodynamic performance, inspections of boundary-layer velocity profile, skin-friction coefficient, and boundary-layer shape parameter plots for the blade shapes representing the design intent and mode 1 were undertaken.

3.2.1 Hub Section

The most significant amounts of manufacturing deviation identified by principal component analysis for the hub section, referred to as mode 1, were an approximate four

percent decrease in both the leading and trailing-edge thicknesses. These deviations translated into the mode 1 blade profile having a mixed-out loss bucket that was approximately a one degree shift of the design intent mixed-out loss bucket towards choking, Figure 3.1. On both the stalling and choking sides of the mode 1 mixed-out loss bucket there was a slight decrease in the bucket's slopes over that of the design intent mixed-out loss bucket; however, this alteration in performance was minor in comparison to the results obtained from the mid-span section. Overall, there is no difference between the mode 1 and design intent aerodynamic performance around minimum loss, while elsewhere mode 1 exhibits only a negligible improvement to performance on the choking side and a minute degradation of performance on the stalling side of the mixed-out loss bucket relative to the design intent.
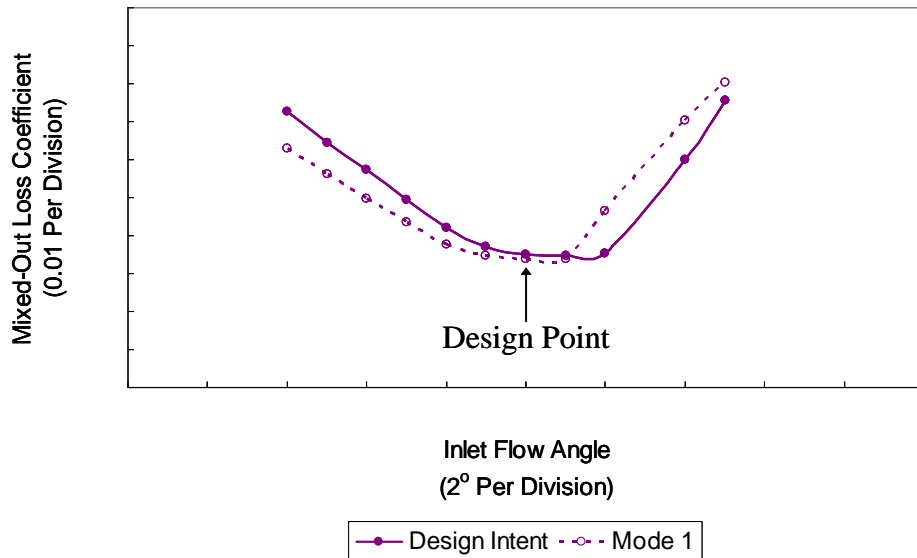
Figure 3.1. Hub section design intent and mode 1 mixed-out loss buckets

3.2.2 Mid-Span Section

The most significant amounts of manufacturing deviation identified by principal component analysis for the mid-span section, referred to as mode 1, were an approximate four percent increase in the leading-edge thickness and an approximate four percent decrease in the trailing-edge thickness. These deviations translated into the mode 1 blade profile having a mixed-out loss bucket that was approximately two degrees narrower than the design intent mixed-out loss bucket, Figure 3.2. On both the stalling and choking sides of the mode 1 mixed-out loss bucket there was no noticeable change to the bucket's slopes over that of the design intent mixed-out loss bucket; however, the narrowing of the mode 1 mixed-out loss bucket was the most significant amount of alteration in aerodynamic performance seen out of the three radial sections investigated. Particularly interesting was the rate and degree with which the mode 1 mixed-out loss bucket deviated from the design intent mixed-out loss bucket as the inlet flow angle moved away from minimum loss and towards stall; this is seen as the inlet flow angle goes from design

10

value of alpha one to the off-design value alpha two. Overall, this was the location at which the greatest amount of manufacturing deviation appeared to have the largest influence on the aerodynamic performance out of the three compressor blade radial sections investigated, and hence a more refined inspection of the compressor blade aerodynamics at this location was conducted.
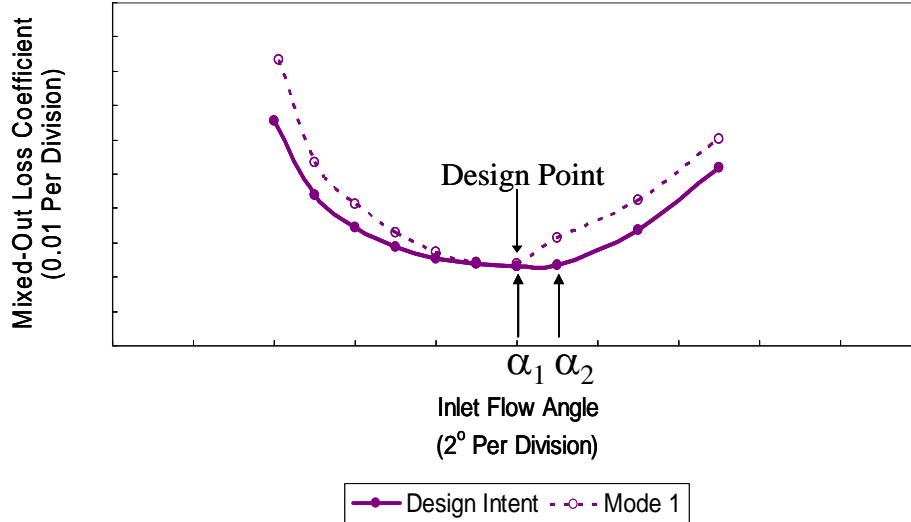
Figure 3.2. Mid-Span section design intent and mode 1 mixed-out loss buckets

The first of the three additional performance parameters inspected were the compressor blade boundary-layer velocity profiles. Inspection of the leading-edge boundary-layer velocity profiles showed no visible difference between the mode 1 and design intent profiles at inlet flow angles of alpha one and alpha two; however, at the trailing edge there was a noticeable difference in the boundary-layer velocity profiles for the design intent and mode 1 at the alpha two inlet flow angle, Figure 3.3. At an alpha two inlet flow angle the mode 1 blade shape suction side displayed the onset of separation and a noticeable increase in boundary-layer displacement thickness over that of the design intent profile, thus indicating that the well attached flow and thinner boundary-layer displacement thickness on the trailing-edge suction side of the design intent profile produces a more desirable mixed-out loss coefficient at the off-design inlet flow angle of alpha two.

To confirm that the trailing-edge region was culpable for the mode 1 aerodynamic performance deterioration, skin-friction coefficient plots of the mode 1 and design intent blade shapes at inlet flow angles of alpha one and alpha two were investigated. Plots of the skin-friction coefficient, Figure 3.4, revealed that although the cause for increases in mixed-out losses can be attributed to the trailing-edge region of the compressor blade, it is the blunter profile and increased thickness of the leading edge that influences the behavior of the trailing-edge boundary layer. This is evident by the flow behavior at the leading edge of the mode 1 blade shape with an inlet flow angle of alpha two; here the initiation of a laminar separation bubble near the leading edge promotes an earlier transition from laminar to turbulent flow in the boundary layer, which increases the skin

11

friction on the surface of the compressor blade and allows for a thicker boundary-layer displacement thickness to be produced downstream.

θ = inlet flow angle $\delta*$ = boundary-layer displacement thickness
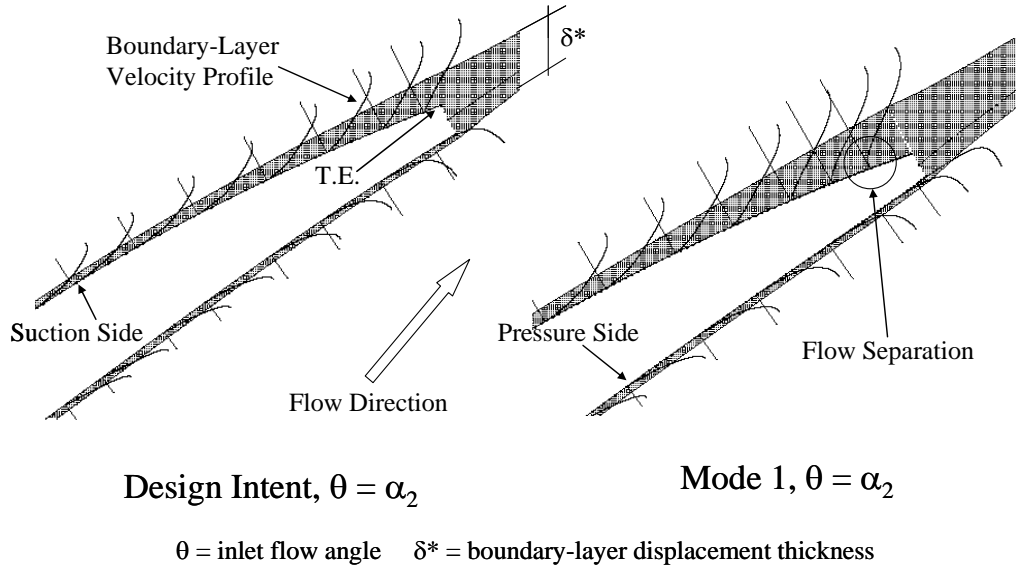
Figure 3.3. Mid-Span section trailing edge boundary-layer velocity profile plots
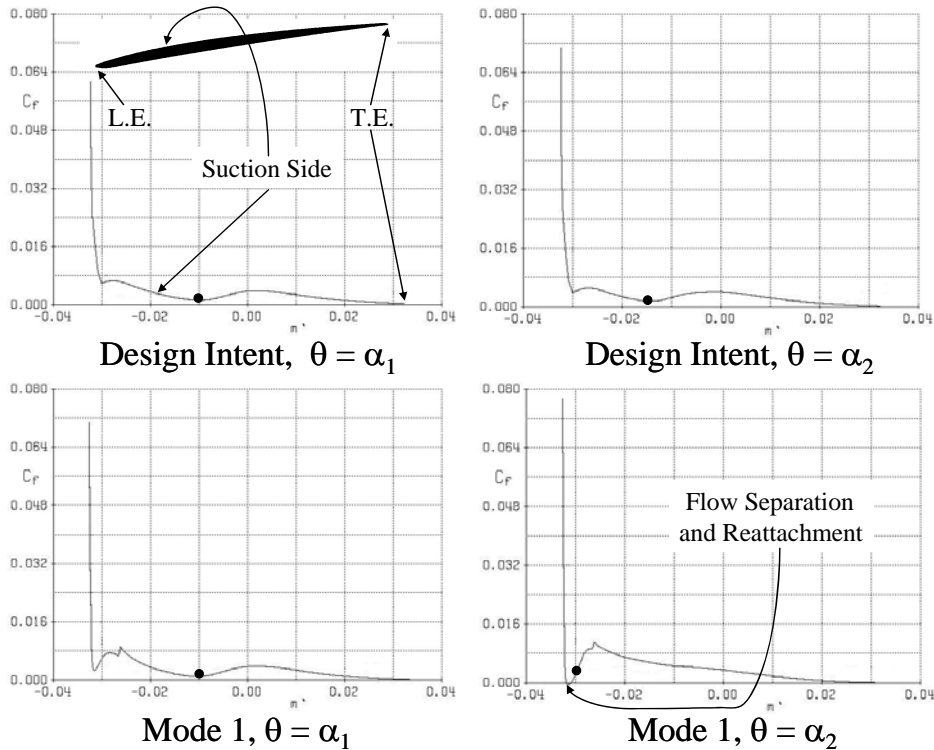
• Laminar to Turbulent Boundary Layer Transition Location

Figure 3.4. Mid-Span section design intent and mode 1 suction side C_f plots

Reaffirmation of the thought that the profile and thickness of the leading edge critically influences downstream boundary-layer behavior was carried out via plots of the boundary-layer shape parameter, defined as the ratio of boundary-layer displacement thickness to boundary-layer momentum thickness, Figure 3.5. An investigation of these plots confirmed that compressor blade aerodynamic performance for given compressor blade shapes at different inlet flow angles is a function of the flow behavior in the leading-edge region of the blade's suction side, this is most notable in the boundary-layer shape parameter plot for mode 1 at an inlet flow angle of alpha two. Here the most significant alteration in performance over the other three boundary-layer shape parameter plots is seen in the form of a larger initial boundary-layer shape parameter spike at the leading edge, which is caused by a significant increase in the initial acceleration of the flow at the leading edge of the compressor blade. This result, in conjunction with the other previously discussed results, indicates that the increases in mixed-out losses incurred by the behavior of the trailing edge boundary layer is a function of the leading edge boundary layer behavior.
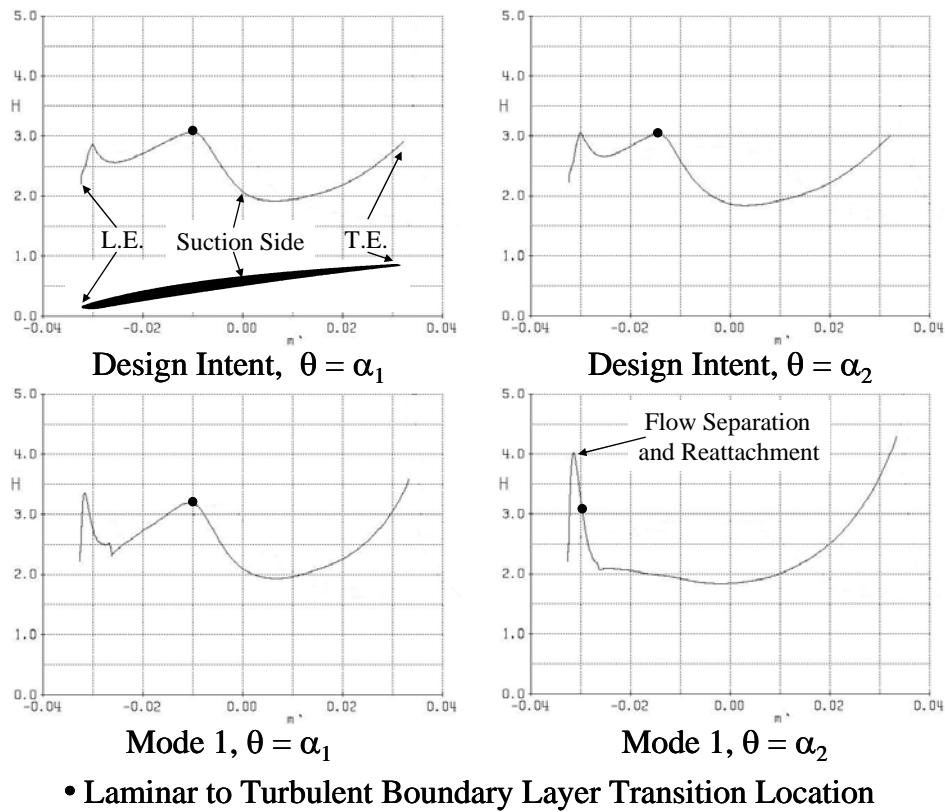
Figure 3.5. Mid-Span section design intent and mode 1 suction side H plots

3.2.3 Tip Section

The most significant amount of manufacturing deviation identified by principal component analysis for the tip section, referred to as mode 1, was an approximate six percent increase in mid-chord thickness. This large deviation in the mode 1 blade profile, over that of the design intent, had a minimal effect on the aerodynamic performance of

13

the compressor blade, Figure 3.6. On both the stalling and choking sides of the mode 1 mixed-out loss bucket there was a slight increase in the bucket's slopes in comparison to the design intent's mixed-out loss bucket; however, this alteration in performance was minor in comparison to the results obtained from the mid-span and hub sections. Overall, there is no significant difference between the mode 1 and design intent aerodynamic performance around minimum loss, while elsewhere mode 1 exhibits only a negligible degradation to performance on the choking and stalling side of the mixed-out loss bucket.
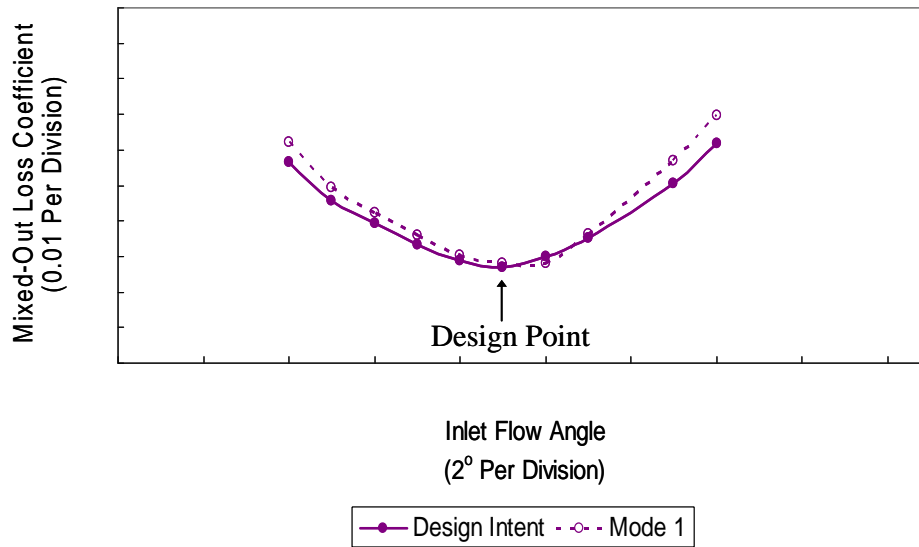
Figure 3.6. Tip section design intent and mode 1 mixed-out loss buckets

3.3 Conclusions

There was no appreciable difference between the mixed-out loss buckets for the design intent and mode 1 compressor blade shapes at the tip section, and the mode 1 mixed-out loss bucket for the hub section only exhibited a slight one degree shift from the design intent mixed-out loss bucket towards choking. The most significant alteration in compressor blade aerodynamic performance was seen at the mid-span section. Here the mixed-out loss bucket for the mode 1 blade shape was two degrees narrower than the design intent mixed-out loss bucket, where the rate and degree with which the mode 1 mixed-out loss bucket deviated from the design intent mixed-out loss bucket as the inlet flow angle moved away from minimum loss and towards stall was of particular interest. Thus, further investigation of the mid-span section through the use of boundary-layer velocity profile, skin-friction coefficient, and boundary-layer shape parameter plots were employed to reveal that the mid-span section's noteworthy deviations in performance were being incurred through alterations to the boundary-layer behavior at the trailing edge of the compressor blade, where these changes emanated from alterations of the boundary-layer flow in the leading-edge portion of the blade's suction surface.

This indication that the leading-edge region is critical to compressor blade performance was previously highlighted in the results of Lamb and Darmofal [1] and Garzon and Darmofal [2], and was further confirmed by the correlations between the

results of this study's numerical and principal component analysis. These results revealed that the radial compressor blade sections with an approximate four percent change in leading-edge thickness and a blunting of the leading-edge elliptical shape, from that of the design intent, experienced the most significant changes in performance. This then makes clear that the worst geometric variations, from an aerodynamic standpoint, are the four percent increase of the leading-edge thickness and blunting of the leading-edge elliptical shape from that of the design intent at the mid-span section, opposed to the four percent decrease in the leading-edge thickness from the design intent at the hub section. However, it must be reiterated that these findings are not completely unexpected, as other previous works, such as that of Roberts et al. [16], have mentioned that compressor blade leading-edge shape plays a pivotal role in determining compressor blade performance and that it is better to err on the side of manufacturing compressor blades with thinner leading-edge thicknesses rather than thicker.

3.3.1 Overview of Two-Dimensional Cascade Aerodynamics

It is important to note, that the term performance used throughout this thesis is in reference to two-dimensional mixed-out loss coefficients. The two-dimensional mixed-out loss coefficients are used to determine how much of the losses in stagnation pressure are due to friction, where in an ideal case the exit stagnation pressure would equal the isentropic stagnation pressure at the exit and the mixed-out losses would be zero. This, however, is not physically possible, but it does allow for the understanding that smaller mixed-out loss coefficients are more desirable. Of course, two-dimensional cascade aerodynamics can only be used to examine the two-dimensional flow field at a given radial section, thus, the flow effects from end wall boundary layers and tip leakage on the overall aerodynamics of the compressor blade can not analyzed and therefore are not included when referring to the term performance in this thesis.

4. CONCLUSIONS

This chapter elucidates the conclusions that can be drawn from this study's quantification of the compressor blade manufacturing deviations present in an individual rotor of an operational core compressor and the effects that those manufacturing deviations have on the compressor blade's performance. Also provided in this chapter is an outline of the continuing work that should be undertaken in light of this paper's results; as well as, a discussion on a method for applying principal component analysis results from one blade shape to another.

4.1 Overall Research Outcomes

This research has undertaken the quantification of manufacturing deviations in as built compressor blades using principal component analysis, and employed the numerical analysis tool MISES to quantify the effects that the greatest manufacturing deviations, referred to as mode 1, have on compressor blade aerodynamic performance.

Results from the principal component analysis revealed that mode 1 for each of the three radial sections investigated represented 55% to 74% of the total as-manufactured deviations, and that all of the as-manufactured deviations for each of the compressor blade geometric parameters investigated were within plus or minus 4% of the design intent; the predominant deviations being: an approximate four percent decrease in the trailing-edge thickness at the hub and mid-span sections, a four percent increase in the leading-edge thickness at the mid-span section, a four percent decrease in the leading-edge thickness at the hub section, and a blunting of the leading-edge elliptical shape at the mid-span section.

The implementation of the numerical analysis tool MISES then revealed that the latter two of these more dominate deviations played critical roles in determining the compressor blade's two-dimensional aerodynamic performance. At the hub section the effect of a four percent decrease in the leading-edge thickness was shown to shift the mode 1 mixed-out loss bucket by one degree from the design intent mixed-out loss bucket towards choking, while the four percent increase in the leading-edge thickness and blunting of the leading-edge elliptical shape at the mid-span section generated a mode 1 mixed-out loss bucket that was two degrees narrower than the design intent mixed-out loss bucket. These performance effects, as well as a more detailed investigation of the mid-span section's two-dimensional mixed-out loss coefficients, through the use boundary-layer velocity profile, skin-friction coefficient, and boundary-layer shape parameter plots, revealed that the aforementioned deviations at the leading edge of the mid-span section at an off-design inlet flow condition induced a premature boundary-layer transition via a leading-edge laminar separation bubble, which then led to the increase of the downstream boundary-layer thickness and losses on the suction surface of the compressor blade.

This indication that the leading-edge region is critical to compressor blade flow behavior was previously highlighted in the results of Lamb and Darmofal [1] and Garzon and Darmofal [2]. The pivotal role that the compressor blade leading edge plays in determining the blade's flow behavior was also elaborated upon by Roberts et al. [16], which stated that it is better to err on the side of manufacturing compressor blades with

thinner leading-edge thicknesses rather than thicker. Thus, with a review of the current literature and the results from this study, it is shown that from an two-dimensional aerodynamic standpoint the most important geometric region of a compressor blade is the leading edge, where thicker leading edges and blunter elliptical leading-edge profiles adversely effect boundary-layer development and overall losses more than thinner leading edges and elliptical leading-edge profiles.

4.2 Future Work

Based on the outcomes of the research undertaken, two major advancements in this field of study can be proposed. First, the implementation of two-dimensional cascade testing to verify the results from the numerical analysis is needed. This will allow not only for greater confidence in the results presented in this thesis but a deeper understanding of the effects that manufacturing deviations have on compressor blade aerodynamic performance. With a firm grip on the effects that manufacturing deviations have on compressor blade aerodynamic performance, the second step in advancing this research is to carryout cascade testing of manufacturing deviations at low Reynolds numbers. Research in this area of low Reynolds number flows in gas turbine compressor appears to be almost nonexistent in the literature. Thus, any knowledge gained from such an endeavor will aid in both compressor design and the development of numerical tools to model low Reynolds number flows in gas turbine compressors.

4.2.1 Expansion of Principal Component Analysis Capabilities

It is not always feasible to have all of the necessary data required, approximately one hundred measured as-manufactured blade profiles [2], to perform principal component analysis on a given set of as-manufactured compressor blades; this is particularly true when attempting to determine what the manufacturing effects on un-manufactured blade profiles may be. Thus, it is highly desirable to have the ability to use previous principal component analysis results for a particular compressor blade shape to infer what the manufacturing effects on other compressor blade shapes may be.

Theoretically, it is plausible that the principal component analysis results for one compressor blade profile could be used to infer what the manufacturing effects on another blade profile would be; however, until further research can validate this theory, the process is assumed to be valid only if two assumptions are satisfied. The first assumption to be satisfied is that the manufacturing process for both blade profiles is identical; this ensures that the mean and variance of the deviations, as captured by principal component analysis for the as-manufactured blades, is accurately described for the to-be manufactured compressor blades. For the satiation of the second assumption, the design intent of both blade profiles must on the same scale or the manufacturing tolerances for the two compressor blade profiles must be on the same scale; in other words, results from compressor blade profiles with six inch chord lengths could only be applied to blade profiles with half inch chord lengths if the relative, and not the actual, manufacturing tolerances are equivalent.

These assumptions may be viewed as inadequate for accurately carrying out the process of using principal component analysis results from one compressor blade shape to infer what the manufacturing effects on other compressor blade shapes may be;

17

however, until further research is carried out, these rational assumptions create an extremely useful tool. The ability to account for how manufacturing deviations will affect compressor blade performance prior to their actual construction and testing greatly aids in the design of modern compressors that push conventional operating limits and ceilings.

APPENDIX A. PRINCIPAL COMPONENT ANALYSIS DETAILS

Appendix A is created as a supplement to the overview of principal component analysis covered in Section 2.1. The supplemental information provided in this appendix elucidates the practical application of principal component analysis, with respect to radial cross sections of gas turbine compressor blades, by providing greater mathematical detail on principal component analysis and information on the Virginia Tech code designed to implement principal component analysis on two-dimensional compressor blade data. Of particular note, is the fact that the overview of the Virginia Tech code is presented in terms of both the code's structure and validation.

A.1 Principal Component Analysis Mathematical Outline

The first task in applying principal component analysis to two-dimensional compressor blade data is to create a p x n data matrix, where n is the number of data sets, number of blades used in the analysis, and p is the number of points, x-y coordinate pairs, that define the shape of the blades in the data sets. With the size and general construct of the data matrix defined, the construction of the data matrix itself can then begin.

First, the x-y coordinate differences between the design intent and the as-manufactured blades are computed. This is done by calculating the error vectors, Eq. A1.1, which is simply the x-y coordinate differences in each data set, from the design intent, for every point p.

$$\mathbf{ER}_{j,i} = \mathbf{MFG}_{j,i} - \mathbf{DESG}_j \qquad \text{Equation (A1.1)}$$

where,

$$\mathbf{MFG}_{j,i} = \begin{bmatrix} x_{1,1} \\ y_{2,1} \\ \vdots \\ x_{2*j-1,i} \\ y_{2*j,i} \end{bmatrix} \quad \text{for} \quad j = 1,\ldots,p \quad \text{and} \quad i = 1,\ldots,n$$

and

$$\mathbf{DESG}_j = \begin{bmatrix} x_{1,1} \\ y_{2,1} \\ \vdots \\ x_{2*j-1,1} \\ y_{2*j,1} \end{bmatrix} \quad \text{for} \quad j = 1,\ldots,p$$

19

Once the error vectors have been calculated, the mean of the error vectors is computed according to Eq. A1.2. The mean of the error vectors are then the mean of the deviation for the entire set of as-manufactured blades n, from the design intent, at every point p.

$$\mathbf{MEAN}_j = \frac{1}{n}\sum_{i=1}^{n} \mathbf{ER}_{j,i} \quad \text{for} \quad j = 1,\ldots, 2p \qquad \text{Equation (A1.2)}$$

After the mean of the error vectors is calculated, it is removed from every set of error vectors, Eq. A1.3, in order to create a set of mean-centered error vectors. The data matrix is then formed by combining the n set of columns containing the mean centered error vectors for every point p, thus yielding the desired p x n data matrix in mean-deviated form.

$$\mathbf{DATA}_{j,i} = \mathbf{ER}_{j,i} - \mathbf{MEAN}_j \quad \text{for} \quad j = 1,\ldots, 2p \quad \text{and} \quad i = 1,\ldots, n \quad \text{Equation (A1.3)}$$

The second task in applying principal component analysis to two-dimensional compressor blade data is to utilize the data matrix to create a covariance matrix, Eq. A1.4 [7-10], where the data matrix used must be in mean-deviated form. Equation A1.4 then produces a symmetric $2p$ x $2p$ matrix, in which the diagonal terms describe the variance in each direction of a x-y coordinate pair p, in relation to every corresponding p in the data set n, and the off-diagonal terms describe the covariance of the x and y dimensions at each point p in the data set n. In other words, the variance is the square of the standard deviation for the x and y components contained in every point p and the covariance describes how x and y vary in relation to each other for every point p.

$$\mathbf{C} = \frac{1}{n-1}\mathbf{XX}^{\mathrm{T}} \qquad \text{Equation (A1.4)}$$

where,

$$\mathbf{X} = [\mathbf{DATA}_{j,1}\,,\ldots, \mathbf{DATA}_{j,n}] \quad \text{for} \quad j = 1,\ldots, 2p$$

Task three in applying principal component analysis to two-dimensional compressor blade data is the calculation of the eigenvalues and eigenvectors for the covariance matrix, which are obtained through the solution of Eq. A1.5 [11]. The desired principle components, for a set of two-dimensional compressor blade data, are then defined as the eigenvectors obtained from the solution of Eq. A1.5, where this solution yields a total of $2p$ principle components and eigenvalues.

$$\mathbf{Cx} = \lambda\mathbf{x} \qquad \text{Equation (A1.5)}$$

The fourth and final task in the application of principal component analysis to two-dimensional compressor blade data is to create the mode vectors, Eq. A1.6, where the mode vectors contain the information required to represent the principal components

and eigenvalues in terms of actual two-dimensional compressor blade shapes in x-y space.

$$\textbf{MODE}_{j,i} = \textbf{DESG}_j + \textbf{MEAN}_j + \lambda\textbf{x}_{j,i} \quad \text{for} \quad i = 1,\ldots, n \quad \text{Equation (A1.6)}$$

where,

$$j = 1,\ldots, p \quad \text{for} \quad \textbf{DESG}_j \quad \text{and} \quad j = 1,\ldots, 2p \quad \text{for} \quad \textbf{MEAN}_j, \ \lambda\textbf{x}_{j,i}, \ \text{and} \ \textbf{MODE}_{j,i}$$

However, in order to make the most efficient use of the mode vectors, the principal components need to be ordered from largest to smallest before employing Eq. A1.6, where the greatest principal component is defined as the eigenvector with the largest eigenvalue and the eigenvector with the smallest eigenvalue defines the smallest principal component. This process of reordering the principal components into a decreasing sequence allows for the easy identification of the largest principal component, where it is the largest principal component that yields the direction in which the scatter of the data is maximized [2]; conversely, the smallest principal component yields the direction in which the scatter of the data is minimized. The largest principal component then reveals the direction in which the standard deviation for every point p in the data set n is the greatest, which in turn can be employed to create a mode vector, via Eq. A1.6. These mode vectors can then be used to construct a two-dimensional compressor blade shape that represents the greatest amount of deviation from the design intent to the as-manufactured blades.

A.2 Principal Component Analysis Code Structure

The code developed at Virginia Tech to perform principal component analysis on two-dimensional compressor blade data is written using the commercially available software MATLAB. Hierarchically, the code is relatively simplistic, due the fact that there are only three main routines: preprocessing of the two-dimensional compressor blade data, implementation of principal component analysis on the aforementioned data, and post processing of the principal component analysis results. Each main routine, however, employs multiple subroutines to complete the main routines required task; a graphical representation of this is provided in Figure A1.

Preprocessing of the two-dimensional compressor blade data is initiated by loading all of the x-y coordinate pairs that define the design intent and as-manufactured blade shapes into the code. Then, the maximal data set, defined as the data set with the greatest number of x-y coordinate pairs, is determined and employed as the basis for creating the new x-y coordinate pairs that will redefine the blade shapes in the remaining data sets. This is crucial, since to carry out the principal component analysis matrix operations, particularly the calculation of the covariance matrix, it is required that every column have the same length. To ensure that every column is identical in length, the x-y coordinate pairs for each data set are splined together; then the splines are decomposed to create a total number of x-y coordinate pairs equivalent to that of the maximal data set. The use of the maximal data set as the basis ensures that no x-y coordinate pairs in any data set are discarded and prevents skewing of the data by decomposing the splines in a

manner, such that, their x-y coordinate pair point densities match that of the maximal data set. Thus, allowing for the reconstructed blade shapes in each data set to be fully defined, and avoiding the possibility of data sets containing blade shapes that are poorly defined at a given location but possess an identical number of x-y coordinate pairs.
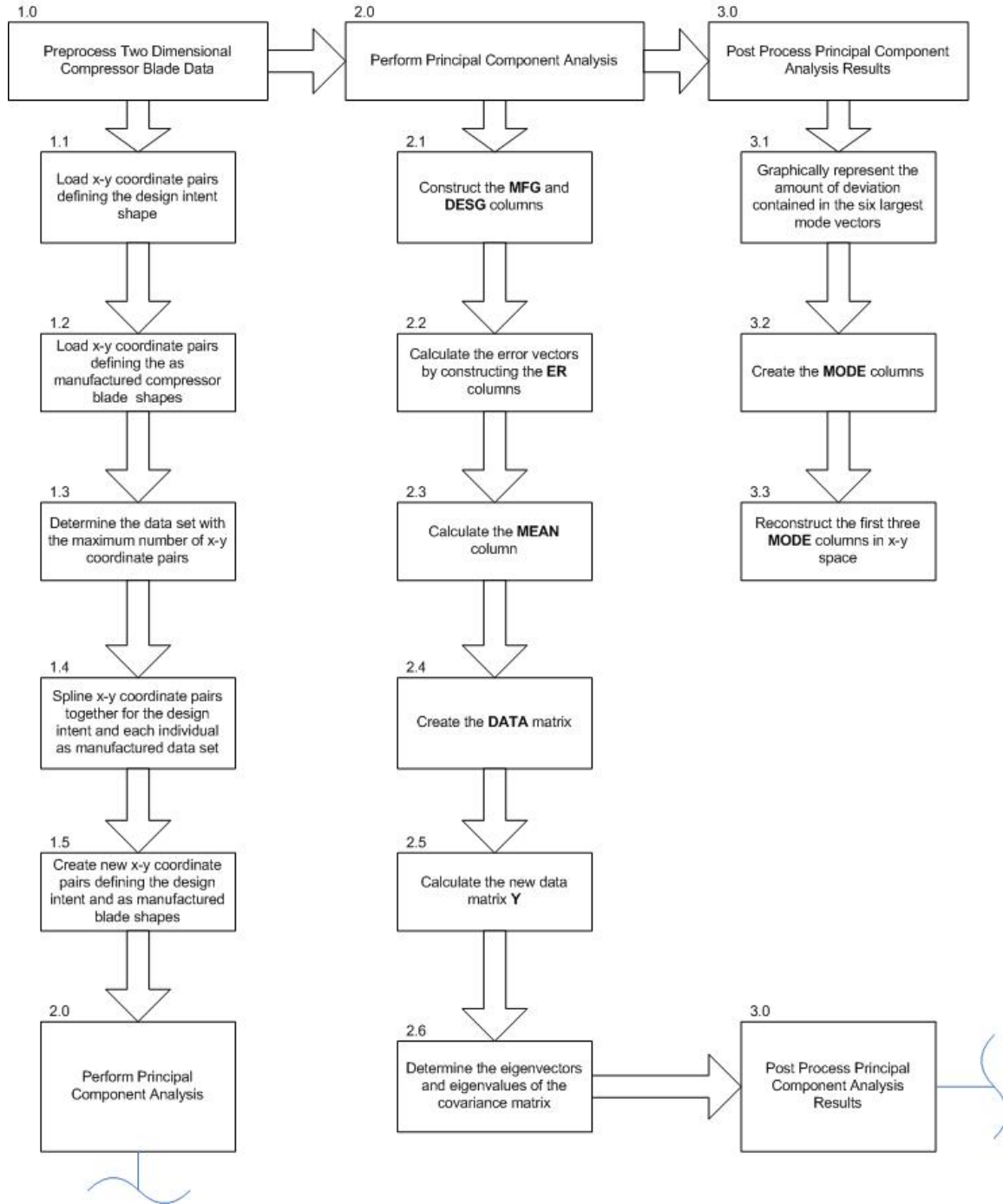
Figure A1. Graphical representation of principal component analysis code

Once all of the two-dimensional compressor blade data sets have been preprocessed, principal component analysis can then be carried out on the data sets. The first step is to simply rearrange the sets of x-y coordinate pairs for each as-manufactured and design intent data set into a single column format, where the column format is defined in Eq. A1.1 of Section A.1 in Appendix A. This then allows the code to systematically carry out Eqs. A1.1-A1.3 of Section A.1 in Appendix A, which correspond to blocks 2.2-2.4 in Figure A1. Determination of the desired eigenvectors and eigenvalues, via Eq. A1.5 in Section A.1 of Appendix A, is then carried out by the code; however, a technique equivalent to principal component analysis, known as singular value decomposition, is employed to compute the principal components.

The use of singular value decomposition, instead of principal component analysis, which can be refereed to as eigenvalue decomposition, is based on the fact that the singular value decomposition of an alternative form of the data matrix is computationally faster than the eigenvalue decomposition of the data matrix's covariance matrix [10]. Implementation of Eq. A2.1 [10] then allows for the creation of the alternate form of the data matrix, where the original data matrix $\mathbf{X}$ retains the definition provided in Eq. A1.4 of Section A.1 in Appendix A.

$$\mathbf{Y} = \frac{1}{\sqrt{n-1}} \mathbf{X}^{\mathrm{T}} \qquad \text{Equation (A2.1)}$$

Singular value decomposition of the alternate form of the data matrix is then carried out via the solution of Eq. A2.2 [17], which is solved using MATLAB's built in function svd [18]. The solution of Eq. A2.2 then provides the desired eigenvectors and eigenvalues of the covariance matrix [17], as defined by Eq. A1.4 in Section A.1 of Appendix A. Where it should be noted, that the substitution of the definition for the alternate form of the data matrix, provided by Eq. A2.1, into Eq. A2.3 proves that the covariance matrices obtained from the data matrix for singular value decomposition and the data matrix for principal component analysis are equivalent.

$$\mathbf{Y} = \mathbf{U}\mathbf{\Sigma}\mathbf{V}^{\mathrm{T}} \qquad \text{Equation (A2.2)}$$

$$\mathbf{C} = \mathbf{Y}^{\mathrm{T}}\mathbf{Y} \qquad \text{Equation (A2.3)}$$

With the solution of Eq. A2.2, it is now possible to post process the singular value decomposition results and analyze the principal components. The first step is to order the principal components from largest to smallest, but this is automatically handled by MATLAB's svd function. Thus, the first true step in the code for post processing is to graphically display the percent variance represented by each of the first six mode vectors, where the percent variance is simply calculated by dividing the square of the desired eigenvalue contained in the diagonal of the $\mathbf{\Sigma}$ matrix by the sum of the squares of the eigenvalues in the diagonal of the $\mathbf{\Sigma}$ matrix. This then allows for the easy identification of how much deviation, due to manufacturing effects, is represented by each individual mode vector. After this is completed, the deviation contained in each of the first three mode vectors is represented by actual two-dimensional compressor blade shapes in x-y space, where each shape is reconstructed using the appropriate mode vector, Eq. A1.6 of

Section A.1 in Appendix A. It should be noted, that despite using singular value decomposition instead of principal component analysis, the aforementioned equation remains valid; the λ and $\mathbf{x}$ matrices are simply replaced by the Σ and $\mathbf{V}$ matrices, respectively. Now, accurately constructed plots of the first three mode vectors allow for the visualization of the most significant amounts of deviation between the as-manufactured blades and the design intent.

A.3 Principal Component Analysis Code Validation

The need for the validation of the code developed at Virginia Tech, which performs principal component analysis on two-dimensional compressor blade data, was twofold. First, it was critical to ensure that implementing the singular value decomposition of the alternative form of the data matrix, opposed to the eigenvalue decomposition of the data matrix's covariance matrix, would not have a deleterious effect on the final results; secondly, code validation was needed to ensure that the code's preprocessing routine would not impart any undesired alteration to the original data set. Two simple test cases, based on altering only the chord length of the rotor's hub section, were employed to carry out the code validation; these test cases are outlined below and consist of using a data set with zero variance and a randomly distributed data set.

A.3.1 Zero Variance Data Set

The zero variance data set test case was the simpler of the two test cases employed, and was intended to primarily test the preprocessing routine of the Virginia Tech code. By implementing principal component analysis on a zero variance data set, it ensured that the deviations returned from the principal component analysis would be equivalent to the mean deviation between the design intent and altered geometry, as long as the preprocessing routine did not inaccurately reconstruct the data set. Creation of the zero variance data set required identical deviations throughout the data set, and obtaining such a data set was accomplished by replicating a single altered geometry 96 times. Construction of the single altered geometry was carried out by using the Rolls Royce blade profile generating code BD76 to scale only the chord length of the hub design intent profile in Section 2.2 by 19.4%.

Implementation of the Virginia Tech code, with the aforementioned zero variance data set, revealed that the preprocessing routine did not impart any undesired alterations to the data set during reconstruction. Evidence of this fact was seen in two of the principal component analysis outputs. First, mode one represented all of the deviation in the data set, which should occur when the scatter of the data is in a single direction; in this case, the direction in which the x-y coordinate pairs were altered to change the chord length of the altered geometry. And secondly, the chord length for mode one was 19.4% greater than that of the design intent, which is equivalent to the mean deviation between the design intent and altered geometry.

A.3.2 Randomly Distributed Data Set

The randomly distributed data set test case was intended to primarily test the substitution of singular value decomposition for eigenvalues decomposition in the Virginia Tech code. By implementing the Virginia Tech code with a known randomly distributed data set, it ensured that the deviations returned from the code would be equivalent to the standard deviation plus the mean of the differences between the design intent and altered geometries, as long as singular value decomposition was a valid substitution for eigenvalue decomposition. Creation of the randomly distributed data set required 96 different altered geometries; all of which were constructed by using the Rolls Royce blade profile generating code BD76 to scale only the chord length of the hub design intent profile in Section 2.2. A random number generator, programmed to output percent scale values from 0 to 20, was used to create the scale factors for each geometry, where the standard deviation plus the mean of the percent scale factor set come out to be 15.9.

Implementation of the Virginia Tech code, with the aforementioned randomly distributed data set, revealed that the substitution of singular value decomposition for eigenvalue decomposition is valid. Evidence of this fact was seen in two of the Virginia Tech code outputs. First, mode one represented all of the deviation in the data set, which should occur when the scatter of the data is in a single direction; in this case, the direction in which the x-y coordinate pairs were altered to change the chord length of the altered geometry. And secondly, the chord length for mode one was 15.6% greater than that of the design intent, which is approximately the standard deviation plus the mean of the deviation between the design intent and altered geometry.

A.4 Virginia Tech Principal Component Analysis Code User Manual

The installation and operation of the Virginia Tech principal component analysis code is provide below, where prior to the installation of the code, it should be noted, that the Virginia Tech principal component analysis code was written for version 7.0 of MATLAB and has not been tested with any other versions of MATLAB.

A.4.1 Virginia Tech Principal Component Analysis Code Installation

Prior to installation it should be noted that the Virginia Tech principal component analysis code is currently installed on the Dell Precision T3400 PC, Virginia Tech barcode VT000306568, located in Room 101 of Randolph Hall and the requisite files to install the code elsewhere are located on the Linux machines in Room 114C of Randolph Hall, where the directory to the files is /home/delosier/ManufacturingTolerances/PCA/ MatLab Program/PCA Section. Once the proper files have been procured they can be used to install the Virginia Tech code by following the two steps outlined below.

1. Create a folder on the hard drive entitled PCA Program.

2. Place the following MATLAB m-files in the newly created folder:
   – Density_Matching_Spliner, Dister, splineWfix, Evaluator, diffplotstring

A.4.2 Virginia Tech Principal Component Analysis Code Operating Instructions

Prior to the operation of the Virginia Tech code the user should have a basic working knowledge of MATLAB. If this is the case, then the following instructions should be a sufficient guide to using the Virginia Tech principal component analysis code.

1. Create a folder on the hard drive entitled PCA Data.

2. Place all of the CMM data and the coordinates of the design intent shape in the newly created folder PCA Data.

   – The CMM data file names are case sensitive and must be named 16008XXXDD.bcon, where the XXX represents the numbers 001-100.

     – Therefore, depending on the number of files you have, you could have files named 16008001DD.bcon thru 16008098DD.bcon, in numerical order.

   – The file containing the data for the design shape must be an excel file named TestData, case sensitive, and the data for the design intent shape must be on a sheet named Master, case sensitive.

3. Open MATLAB and ensure that the Current Directory, Command History, Command Window, and Workspace windows are open.

   – These windows can be turned on/off by going to Display in the menu bar and checking/un-checking the appropriate item.

4. Set a path in MATLAB to the PCA Program folder created during the installation process.

   – In the menu bar go to File > SetPath… and click on the Add Folder… tab.

     – Browse to the folder PCA Program, the one created during installation, and click OK.

   – Make sure the path to the PCA Program folder shows up in the MATLAB search path window.

   – Click on the Save tab and then click the Close tab.

5. Place the CMM data and the coordinates of the design intent shape in the Current Directory window.

   – Click on the … tab in the toolbar, located next to the dialog box that contains the current path to the Current Directory, and browse to the folder PCA Data.

   – Click the OK tab.

6. Clear the Command Window.

   – Type clc and then enter in the Command Window.

7. Clear the entire Command History.

– Right click in the Command History window and select Clear Entire History.

8. Clear the Workspace.

– Highlight all of the items in the Workspace and click on the delete icon in the Workspace toolbar.

9. Run the Virginia Tech code by typing Evaluator, case sensitive, in the Command Window and hitting enter.

10. The Virginia Tech code should start running, the word busy appears in the bottom left corner of the MATLAB display while the program is running.

11. Once the Virginia Tech code is finished running it will display five figures.

– One figure will display the percent of geometric variation each mode contains.

– One figure will display the splined design intent and the CMM data set with the greatest number of points.

– The other three figures will display the shape of the design intent overlaid with either modes 1, 2, or 3.

12. In the Workspace click on the save icon and save all of the results to a .mat file.

APPENDIX B. DETAILS ON MISES SIMULATIONS

Appendix B is created to show the gird independence of the I-Grid used for the MISES simulations in Section 3.2; data for the grid independence study is provided in the form of grid sizes and their corresponding performances.

B.1 MISES I-Grid Independence Results

The I-Grid independence study outlined in this section is based on the blade geometry of the mid-span section design intent. Three different gird sizes were used for this study, as outlined in Table B1. The girds used were classified as course, normal, and fine, with each grid being approximately twice as dense as its predecessor. All of the grids in the I-Grid independence study were non-uniform and used leading and trailing edge spacings of 0.05 and 1.0 respectively.

The results of the I-Grid independence study are given in the form of mixed-out loss buckets, Figure B1. Plots of the mixed-out loss buckets for the three grids investigated revealed that their losses were typically within five percent of one another. Results from the coarse gird did deviate from being within five percent of the other grids as twice minimum loss was approached, here the coarse grid losses were approximately ten percent greater than the other two grids.

Overall, due to the speed at which MISES reaches a converged solution, either the normal or fine gird could have been used without penalty; however, it was decided that the normal gird be used for all MISES simulations. Use of the normal grid, opposed to the fine grid, helped to ensure that no error in constructing the complete computational domain would occur for any given geometry, as MISES does have a limit on the size of the entire computational domain.
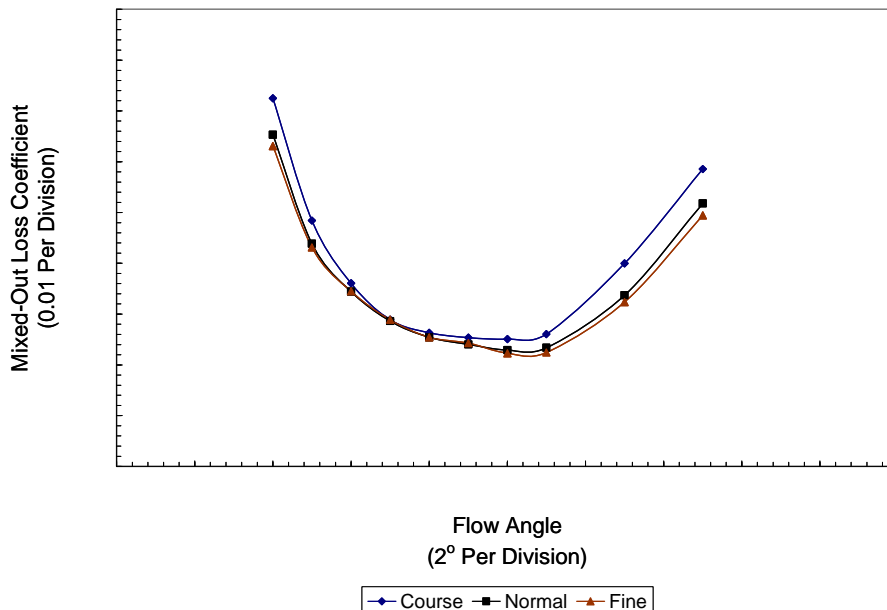

Figure B1. Mixed-Out loss buckets for MISES I-Grid independence study

Grid Description	Number of Grid Points	L.E. Spacing	T.E. Spacing
Course	26	0.05	1.0
Normal	53	0.05	1.0
Fine	106	0.05	1.0

Table B1. Grid parameters for MISES I-Grid independence study

B.2 Overview of Running MISES on Virginia Tech's Linux Machines

The following instructions are meant to serve as a basic guide on how to run MISES on the Virginia Tech Linux machines located in Room 114C of Randolph Hall, and they are not intended as a substitute for the MISES manual located in the /home/delosier/TOOLS/MISES_Source/Mises/doc directory of the aforementioned Linux machines.

B.2.1 File and Directory Setup for the Execution of MISES Cases

This section covers the files required and the file structure needed to run MISES on the Linux machines located in Room 114C of Randolph Hall, where it should be noted, further detail on the format of the required files can be found in Sections B.2.4 to B.2.6 of this Appendix and in the MISES manual located in the /home/delosier/TOOLS/ MISES_Source/Mises/doc directory of the aforementioned Linux machines.

1. Create a folder to hold the solutions for the MISES runs.
   - This folder's title should be descriptive of the case to be run.
2. Create the blade and ises files.
   - Ensure that the blade and ises files have the same *casename*, as MISES will only run if this is the case.
   - The blade file mainly contains information for the blade geometry being used; a sample file and some basic explanation is given in Section B.2.4 of this Appendix.
   - The ises file will contain information on various options for running MISES; a sample file and some basic explanation is given in Section B.2.5 of this Appendix.
3. Place the blade and ises files in the folder created in step one of this section.
   - If the files were created on a Windows based machine then convert them to a Linux format once they are transferred to the Linux machine; this can be done by using the following case and format sensitive command:
     - dos2unix *"name of files, separated by a space, to be converted"*

4. To run multiple MISES cases for a single blade profile on a single mesh, such is the case when creating loss buckets, create the additional folders Increase and Decrease in the same directory as the folder created in step one of this section.

   – This step and those that follow can be ignored if the only interest is running a single MISES case.

5. Create two spec files.

   – Ensure that the spec files have the same *casename* as the blade and ises files created in step two of this section, as MISES will only run if this is the case.

   – The spec file will contain information on the additional flow angles to be run; a sample file and some basic explanation is given in Section B.2.6 of this Appendix.

6. Place the respective spec files for increasing and decreasing flow angles in the Increase and Decrease folders created in step four of this section.

   – If the files were created on a Windows based machine then convert them to a Linux format once they are transferred to the Linux machine; this can be done by using the following case and format sensitive command:

      – dos2unix *"name of files, separated by a space, to be converted"*

B.2.2 Execution of MISES Cases

1. From the folder created in step one of the previous section, run MISES by pointing to following file:

   – /home/delosier/TOOLS/MISES_Source/Mises/run

2. Enter the *casename* of the ises file created in step two of the previous section.

3. Choose option four.

4. In the new window choose option two.

   – Setup the mesh by using the appropriate options; options D and N are usually sufficient.

5. Choose option three.

6. Choose option four.

7. Exit the window by entering zero.

8. Choose option one.

   – Enter the desired number of iterations; fifteen to twenty is usually sufficient.

9. After convergence is reached enter zero for the number of iterations.

10. If convergence is not satisfied the case either needs to be run for a greater number of iterations or an investigation into why the case did not converge needs to be carried out.

   - This is a judgment called based on the user's interpretation of the solutions behavior.

11. If convergence is satisfied the following two actions can be taken:

   - Move on to the post processing of the data.

   - Setup and run additional MISES cases based on the solution of the current case, as is done when creating loss buckets.

12. To run the additional MISES cases needed for creating a loss bucket, copy all of the files from the folder created in step one of the previous section to the folders created in step four of the previous section.

13. From the Increase folder created in step four of the previous section, run MISES by pointing to following file:

   - /home/delosier/TOOLS/MISES_Source/Mises/run

14. Enter the *casename* of the ises file created in step two of the previous section.

15. Choose option 7.

16. After convergence is reached enter zero to exit MISES.

   - If convergence is not satisfied an investigation into why the case did not converge needs to be carried out.

17. Repeat steps thirteen to sixteen for the Decrease folder created in step four of previous section.

B.2.3 Post Processing of MISES Cases

1. The post processing for a single MISES case is done using MISES, where the appropriate options in the main window of MISES are used to perform the desired post processing.

   - The polar files created by steps twelve to seventeen in the previous section are used to post process multiple MISES cases, as is the circumstance when creating loss buckets.

2. Copy the folders created in step four of Section B.2.1 to a Windows based machine; this will allow Excel to be used to complete the post processing.

3. In an Excel file read in the polar files located in the Increase and Decrease folders.

   - Make sure that the files are opened using the Fixed width option and that all columns have a break line between them.

4. Plot any values that are deemed appropriate.

- Typically, a loss bucket is plotted with just the loss coefficients, omega, and inlet flow angles, Sinl.

  - Before plotting loss buckets it is recommended that Sinl be converted back into degrees.

B.2.4 Overview of MISES blade Files

A MISES blade file, which will have the name blade.*casename*, can be created manually or by using the Excel file Blade File Setup Tool located in the directory /home/delosier/ManufacturingTolerances/CFD on the previously mentioned Linux machines. Use of the Blade File Setup Tool is relatively self explanatory; the Blade.xxx Output sheet contains the blade file in the correct format and is populated by providing the appropriate inputs on the Blade Input Parameters sheet. Of particular note, is that part of the blade's trailing edge must be excluded before the blade coordinates are entered into the Blade Input Parameters sheet and the blade coordinates must be ordered from the trailing edge on one side of the blade to the trailing edge on the other side. Further information on the format of the blade files can be found in the MISES manual located on the aforementioned Linux machines.

```
DesignA44
0.96569 0.41872 0.09432 0.09432 0.06545
0.03932576     0.01718619
0.03917879     0.01712863
0.03784848     0.01669087
0.03652424     0.01623948
0.03520303     0.01577596
0.03388636     0.01530032
```

B.2.5 Overview of MISES ises Files

A sample of a typical ises file is given below, where ises files are named ises.*casename*. Typically, the sample ises file provide below is sufficient for running most compressor blade profiles that are operating around the lower end of the transonic region, where only the appropriate values on lines three and four and the corrected Reynolds number on line six would need to be adjusted from case to case. Further explanation on the format of the ises file and other MISES solver options can be found in the MISES manual located on the aforementioned Linux machines.

```
1 2 5
1 4 3
0.69 0 0.96569 -0.11098
0 0 0 0.11539
0 0
1.14e6 -4.0
1.0 1.0
4 0.98 1.0
0 0
0 0 0 0
```

B.2.6 Overview of MISES spec Files

      A MISES spec file, which will have the name spec.*casename*, can be created manually or by using the Excel file Blade File Setup Tool located in the directory /home/delosier/ManufacturingTolerances/CFD on the previously mentioned Linux machines. Use of the Blade File Setup Tool is relatively self explanatory; the Spec.xxx Output Increase and Spec.xxx Output Decrease sheets contain spec files in the correct format, where each sheet contains a spec file for increasing and decreasing flow angles, respectively. Population of both sheets is carried out by providing the appropriate inputs on the Spec Input Parameters sheet. Of particular note, is that the second column in the spec file tells MISES when to write out an idat file, where the names in the second column are appended to the spec file *casename* to identify the idat file. Further information on the format of the spec files can be found in the MISES manual located on the aforementioned Linux machines.

```
1
0.96569
0.95729
0.94896
0.94071
0.93252 43
0.92439
0.91633
0.90834
0.90040 42
0.89253
0.88473
0.87698
0.86929 41
0.86166
0.85408
0.84656
0.83910 40
```

APPENDIX C. DETAILS ON ADPAC SIMULATIONS

As outlined in Section 3.1, it was determined that MISES was a more suitable numerical simulation tool for the work carried out in this research; however, to provide a comprehensive picture the initial ADPAC studies are presented in this appendix. The APDAC studies are presented in two sections: the first section outlines the necessary parameters and boundary conditions for each numerical simulation and the second section presents the parameters and results of an H-Grid independence study.

C.1 ADPAC Simulations

Several ADPAC cases were run for the H-Grid independence study and initial numerical simulations, all of these cases were based on the same set of solver constraints and boundary conditions. The solver constraints consisted of a standard multi-grid scheme and a Baldwin-Lomax turbulence model, use of the algebraic Baldwin-Lomax turbulence being more feasible than the one equation Spalart-Allmaras turbulence model for the initial numerical studies. Boundary conditions were set for both of the blade surfaces, the inlet plane to the blade passage, and the blade passage exit plane. The blade surfaces were treated with a solid surface viscous no-slip boundary condition, while the axial distance from the blade to both the inlet and exit planes had a solid surface inviscid no-through-flow boundary condition to allow for symmetric modeling of the flow passage. For the exit plane a turbomachinery exit boundary condition was employed, while a turbomachinery inflow boundary condition was used for the inlet plane flow conditions of Mach number equal to approximately 0.7 and a Reynolds number of approximately 6.5×10^5. Implementation of ADPAC with the aforementioned constraints and boundary conditions, in conjunction with the operating parameters for the investigated blades, facilitated the creation of the mixed-out loss buckets used in the initial numerical simulations and the proceeding H-Grid independence test.

C.2 H-Grid Independence Study

The H-Grid independence study outlined in this section is based on the blade geometries for the design intent and mode 1 at the mid-span section. Four different gird sizes were used for this study, as outlined in Table C1. The girds used were classified one through four, with gird two being used as the baseline grid. All of the other grids were created by varying one of the baseline grid's parameters; this yielded various non-uniform grids that varied the grid densities at the leading and trailing edges and near the blade surfaces.

The results of the H-Grid independence study are given in the form of mixed-out loss buckets, Figures C1 and C2. Plots of the mixed-out loss buckets for the four grids investigated revealed that the losses of girds three and four were typically within five percent of one another, while grid two was typically within ten percent of grids three and four. Results for gird one were always significantly larger then the other three grids, thus, ruling it out as possibly being grid independent.

Overall, either gird three or four could have been deemed to be grid independent; however, it was decided that gird four be used for all ADPAC simulations. Use of grid

four, opposed to grid three, helped to decrease run time by allowing for fewer total grid points to be used in the entire computational domain.
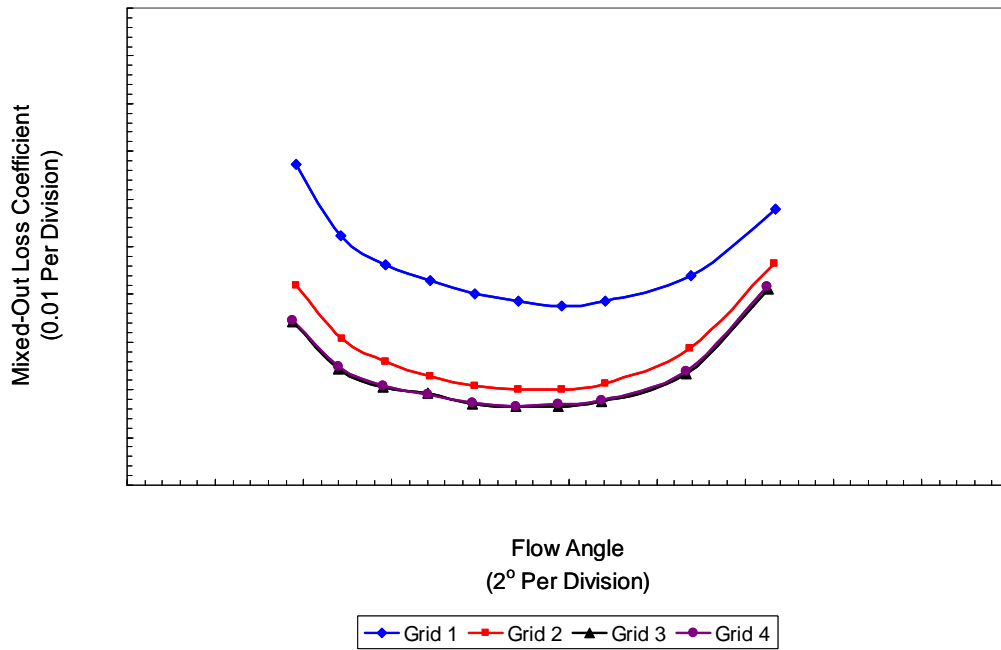
Figure C1. Design intent mixed-out loss buckets for H-Grid independence study
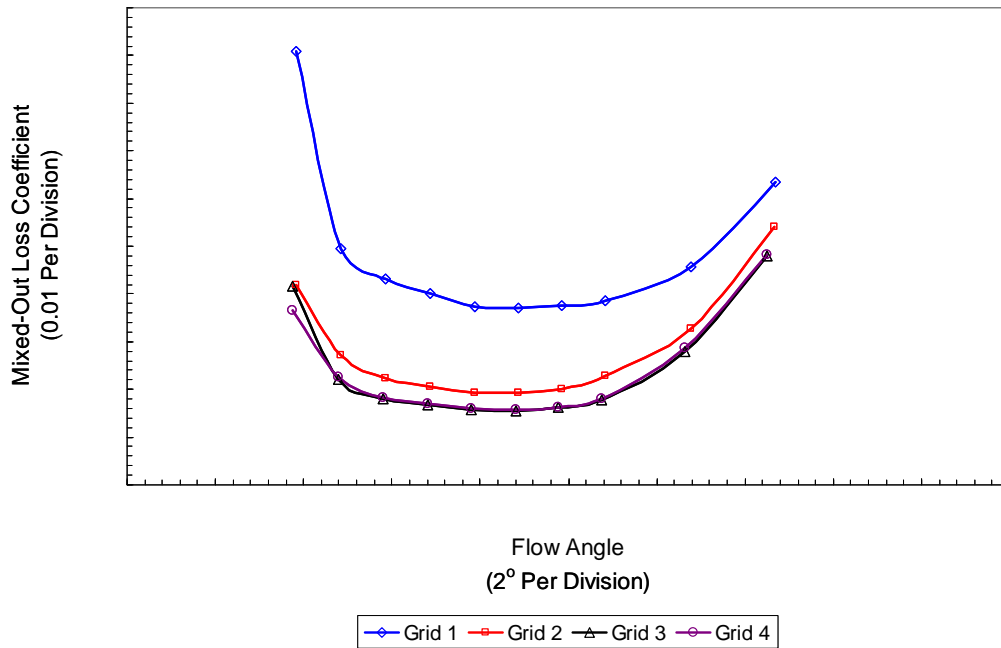
Figure C2. Mode 1 mixed-out loss buckets for ADPAC H-Grid independence study

Grid Description	NBLPTT	NBLPTZ	NBLPKZ
1	69	53	13
2	45	53	13
3	45	97	13
4	45	53	19

Table C1. Grid parameters for ADPAC H-Grid independence study
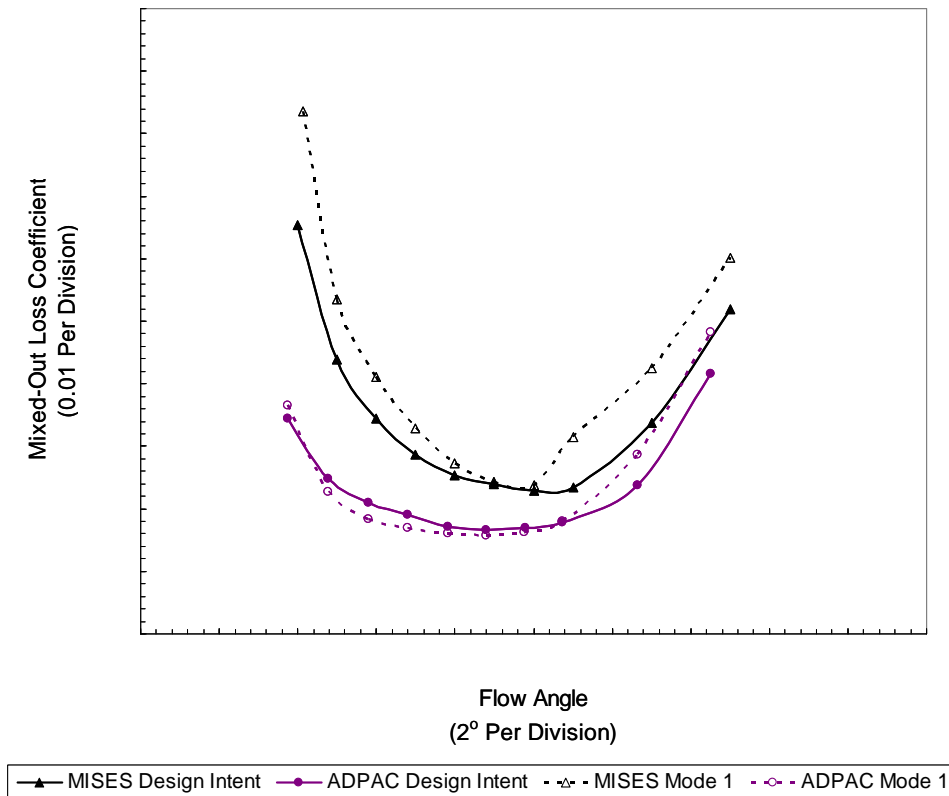
Figure C3. MISES and APDAC Mixed-Out Loss Bucket Comparison

C.3 Overview of Running ADPAC on Virginia Tech's Linux Machines

The following instructions are meant to serve as a basic guide on how to run ADPAC on the Virginia Tech Linux machines located in Room 114C of Randolph Hall, and they are not intended as a substitute for the ADPAC manual located in Room 101 of Randolph Hall. This brief tutorial is also not intended to cover the process of mesh generation for ADPAC cases, as several software options, such as Gridgen and Mulac, exist for this task; further information on using Mulac is given the file MulacInfo, which

is located on the Linux machines in Room 114C of Randolph Hall under the directory /home/delosier/ ManufacturingTolerances/CFD.

C.3.1 File and Directory Setup for the Execution of ADPAC Cases

This section covers the files required and the file structure needed to run ADPAC on the Linux machines located in Room 114C of Randolph Hall, where it should be noted, further detail on the format of the required files can be found in Sections C.3.4 and C.3.5 of this Appendix and in the ADPAC manual located in Room 101 of Randolph Hall.

1. Create two folders entitled Geom and Solutions.

2. In the Geom folder place the mesh file *casename*.mesh.

3. In the Solutions folder create another folder to hold the solutions for the ADPAC runs.

    – This folder's title should be descriptive of the case to be run.

4. Create the boundata and input files using the Linux program nedit.

    – Ensure that the mesh, input, and boundata files all have the same *casename*, as ADPAC will only run if this is the case.

    – The boundata file will contain information on the boundary conditions for the mesh, where a sample file and some basic explanation is given in Section C.3.4 of this Appendix.

    – The input file will contain information on various options for running ADPAC; a sample file and some basic explanation is given in Section C.3.5 of this Appendix.

5. Place the boundata and input files in the folder created in step three of this section.

6. In the folder created in step three of this section, create a symbolic link to the file *casename*.mesh located in the Geom folder.

7. To run multiple ADPAC cases for a single blade profile on a single mesh, such is the case when creating loss buckets, create additional folders for every flow angle of the loss bucket in the Solutions folder.

    – This step can be ignored if the only interest is in running a single ADPAC case.

C.3.2 Execution of ADPAC Cases

1. From the folder created in step three of the previous section, run ADPAC by using the following case and format sensitive command:

    – adpac_linux_mpich1.s2 <*casename*.input> *casename*.output

37

2. After the ADPAC case stops running the convergence of the solution can be checked by one of two following methods:

   – Look at the last few iterations for mass in, mass out, rms error, and max error using the following case and format sensitive command:

     – tail *casename*.output

   – Graphically display the residuals using the following case and format sensitive command:

     – sh.jacc_converge *casename*.converge

3. If convergence is satisfied the following two actions can be taken:

   – Move on to the post processing of the data.

   – Setup and run additional ADPAC cases based on the solution of the current case, as is done when creating loss buckets.

4. If convergence is not satisfied the case either needs to be run for a greater number of iterations or an investigation into why the case did not converge needs to be carried out.

   – This is a judgment called based on the user's interpretation of the solutions behavior.

5. To run the additional ADPAC cases for creating a loss bucket, the new emdot and pexit, mass flow rate and exit pressure values, for each new case to be run must be determined, as these change as flow angle changes.

   – Open the newly created file *casename*.output

   – Find the final pexit and emdot values and use them as a basis for what the values of pexit and emdot need to be for the new cases to be run.

     – Typically as flow angle increases the emdot value needs to be decreased and the pexit value needs to be raised, where the inverse is true for a decrease in flow angle.

6. After the emdot and pexit values for the new cases have been determined, the new input and boundata files can be created. This is done using the following case and format sensitive command from the Solutions folder created in step one of the previous section:

   – sh.setuprestarts_single "*name of the folder created in step three of the previous section*" "*names of the folders, separated by a space, created in step seven of the previous section*"

     – It should be noted, that only nine additional folders can used per command.

7. Change each input file by: changing the number iterations to an appropriate value, turning the multi-grid scheme off, and turning the restart function on.

   – Make sure to save the nedit file before closing it.

8. Change each boundata file by: changing the inlet flow angle and changing the pexit and emdot values to those that were determined in step five of this section.

   – Make sure to save the nedit file before closing it.

9. Run all of the newly created ADPAC cases from the Solutions folder created in step one of the previous section by using the case and format sensitive command:

   – sh.runrestarts_single *"the names of the folders, separated by a space, created in step seven of the previous section"*

10. After the ADPAC cases stop running, their convergence can be checked by using the case and format sensitive command from the Solutions folder created in step one of the previous section:

   – sh.checkcases_single *"the names of the folders, separated by a space, created in step seven of the previous section"*

11. If convergence is satisfied then post processing can begin, and if convergence is not satisfied then see step four of this section.

C.3.3 Post Processing of ADPAC Cases

1. To reduce the data for a single ADPAC case run the following case and format sensitive command from the Solutions folder created in step one of Section C.3.1:

   – sh.reducedata_single *"name of the folder created in step three of Section C.3.1"*

2. To reduce the data for multiple ADPAC cases run the following case and format sensitive command from the Solutions folder created in step one of Section C.3.1:

   – sh.reducedata_single *"the names of the folders, separated by a space, created in steps three and seven of Section C.3.1"*

3. Copy the entire directory created in step one of Section C.3.1 to a Windows based machine; this will allow Excel to be used to complete the post processing.

4. Open the Excel file ConvHistory and read in the desired ADPAC case file *casename*.converge using the Get NewFile tab.

   – The Excel file ConvHistory is located on the Linux machines in Room 114C of Randolph Hall in the directory /home/delosier/Manufacturing Tolerances/CFD

5. Change the Iterations field to a value of 100 and copy the value in the PR field.

   – Paste the PR field value into an Excel file that will be used to plot and display all of the pertinent data from the APDAC solution.

6. Use Excel to open the desired ADPAC case file ax01.le located inside the Axi folder, which is inside the corresponding ADPCA case folder created in step three or seven of Section C.3.1.

  – Copy the Mach numbers to the same Excel file used in step five of this section.

    – The average of the Mach numbers is typically the Mach number for a two-dimensional case.

  – Make sure that the file is opened using the Fixed <u>w</u>idth option and that all columns have a break line between them.

7. Use Excel to open the desired ADPAC case file bep01 located inside the Bep folder, which is inside the corresponding ADPAC case folder created in step three or seven of Section C.3.1.

  – Copy all of the desired values to the same Excel file used in step five of this section.

    – Typical useful parameters are LossCoef#, Beta 1#, and Beta 2#, which are the mass averaged loss coefficient, inlet flow angle, exit flow angle, respectively.

    – The average values of the aforementioned parameters or any other parameter in the bep01 file are typically the values for a two-dimensional case.

  – Make sure that the file is opened using the Fixed <u>w</u>idth option and that all columns have a break line between them.

8. Repeat steps four thru seven in this section for post processing more than one ADPAC case, as would be the situation when creating loss buckets.

  – Plot loss coefficient versus inlet flow angle to create the desired loss bucket.

C.3.4 Overview of ADPAC boundata Files

A sample of a typical boundata file is given below, where boundata files are named *casename*.boundata. Lines that begin with the pound sign are commented lines and do not effect the way the boundata file is read. The lines that begin with a phrase, such as INLETT, followed by a string of letters and numbers, define specific types of boundary conditions, where the available boundary conditions and the method for applying them are given in the ADPAC manual located in Room 101 of Randolph Hall. Of particular note, the columns of additional information for some of the boundary conditions are a necessary part of that boundary conditions definition; further detail of these boundary conditions can of course be found in the aforementioned ADPAC manual.

```
#----------------------------------------------------------------------
# ADPAC BOUNDATA FILE
# CASENAME example
#----------------------------------------------------------------------
```

```
#
#-> INLET CONDITIONS
#
INLETT   1 1 I I P P J K  1  1  1  5  1 69  1  5  1 69
 NDATA
   3

 68.50084  1.00000  1.00000  0.00000 47.00000
 68.00018  1.00000  1.00000  0.00000 47.00000
 68.69952  1.00000  1.00000  0.00000 47.00000


#
#-> EXIT CONDITIONS
#
EXITT    1 1 I I M M H H 109 109  1  5  1 69  1  5  1 69
   PEXIT        EMDOT        PRELAX
  0.8100        0.0896       0.05


#
#-> PATCH: LOWER-TO-UPPER, UPSTREAM
#
PATCH    1 1 K K P M I J  1 69  1 29  1  5  1 29  1  5


#
#-> PATCH: UPPER-TO-LOWER, UPSTREAM
#
PATCH    1 1 K K M P I J 69  1  1 29  1  5  1 29  1  5


#
#-> PATCH: LOWER-TO-UPPER, DOWNSTREAM
#
PATCH    1 1 K K P M I J  1 69 81 109  1  5 81 109  1  5


#
#-> PATCH: UPPER-TO-LOWER, DOWNSTREAM
#
PATCH    1 1 K K M P I J 69  1 81 109  1  5 81 109  1  5


#
#-> UPPER AND LOWER INVISCID SURFACES
#
SSIN     1 1 J J P P I K  1  1  1 109  1 69  1 109  1 69

SSIN     1 1 J J M M I K  5  5  1 109  1 69  1 109  1 69


#
#-> SUCTION-SIDE AND PRESSURE-SIDE BLADE VISCOUS SURFACES
#
SSVI     1 1 K K P P I J  1  1 29 81  1  5 29 81  1  5
   RPMWALL      TWALL
    0.000000    0.000000
SSVI     1 1 K K M M I J 69 69 29 81  1  5 29 81  1  5
   RPMWALL      TWALL
    0.000000    0.000000
```

```
#
#-> END OF BOUNDATA FILE
#
ENDDATA
```

C.3.5 Overview of ADPAC input Files

A sample of a typical input file is given below, where input files are named *casename*.input. Lines that begin with the pound sign are commented lines and do not effect the way the input file is read. The explanations that follow some of the lines, such as those in the START UP section, are part of the code. These explanations give guidance on what values must be used in order to use specific functions of the ADPAC code; further explanation of these functions and a more detailed description of the input file can be found in the ADPAC manual located in Room 101 of Randolph Hall. It should also be noted, that the full multi-grid trigger should only be used for a start-up run and should be turned off for a re-start run.

```
#---------------------------------------------------------------------
# Rotor H-Grid
# ADPAC Input File
#---------------------------------------------------------------------

#
#-> SETUP
#
CASENAME   =  sample
FCART      =      0.0
DIAM       =      0.083333
FMULTI     =      3.0
FNCMAX     =    500.0
FITCHK     =    100.0
NBLD(1)    =    960.0
RPM(1)     =      0.000000
RPM(2)     =      1.000000


#
#->START UP
#
FFULMG   =    1.0    full multigrid trigger (used to start solution), =0.0 standard multigrid, =1.0 full
                     mulitigrid; default <1.0>
FCOAG1   =    3.0    coarsest coarse mesh level upon which the "full" multigrid is initially applied;
                     default <1.0> (typically set to f_multi)
FCOAG2   =    2.0    finest coarse mesh level upon which the "full" multigrid calculation is applied;
                     default <2.0>
FITFMG   =  100.0    number of iterations on each coarse level of multigrid during full multigrid
                     startup; defualt <100.0>
FREST    =    1.0    restart trigger, =0.0 not a restart, =1.0 restart; default <0.0>
FSUBIT   =    3.0    number of subiterations on coarse mesh during coarse mesh portion of multigrid
                     cycle (between 1.0 ~ 3.0); default <1.0>


#
#-> CONSTANTS
#
GAMMA    =  1.400000
```

```
PREF        =    13104.000000
RGAS        =    1716.260010
RMACH       =    0.500000
TREF        =    923.600000


#
#-> SPACING AND TURBULENCE MODEL
#
CCP         =    1.6      <1.0
CKLEB       =    0.3      <0.64
F1EQ        =    0.0       one equation Spalart-Allmaras turbulence model, =0.0 disables, =1.0 enables;
                          default <0.0>
F2EQ        =    0.0      two equation k-R turbulence model, =0.0 disables, =1.0 enables, if both =0.0
                          Baldwin-Lomax turbulence model; default <0.0>
FINVVI      =    1.0      inviscid trigger, =0.0 inviscid flow, =1.0 viscous flow (does not affect b.c.);
                          default <0.0>
FKINF       =    20.0     control for turbulence model, if f_1eq = 1.0 represents chi ~20, if f_2eq = 1.0
                          represents k field ~0.0001; default <0.0001>
FWALLF      =    0.0       wall function trigger for use in Baldwin-Lomax and 1eq turb. model*!; default
                          <1.0>


#
#->RESIDUAL SMOOTHING SCHEME TRIGGERS
#
EPSX        =    1.000000    residual smoothing constant in i direction; default <1.0>*
EPSY        =    1.000000    residual smoothing constant in j direction; default <1.0>
EPSZ        =    1.000000    residual smoothing constant in k direction; default <1.0>


#
#->TIME CONSTANTS
#
CFL         =    -5.0     <0.0 steady flow, >0.0 unsteady flow (time step factor -- consult manual);
                          default <-5.0>
CFMAX       =    2.0


#
#-> END OF INPUT FILE
#
ENDINPUT
```

REFERENCES

1. Lamb, C.T. and Darmofal, D.L., 2004, "Performance-Based Geometric Tolerancing of Compressor Blades", ASME Paper No. GT2004-53592, *Proceedings of the ASME Turbo Expo 2004: Power for Land, Sea, and Air*, Vienna, Austria

2. Garzon, V.E. and Darmofal, D.L., 2003, "Impact of Geometric Variability on Axial Compressor Performance", *ASME Journal of Turbomachinery*, Vol. 125, pp. 692-703

3. Burton, S.A., Kolonay, R.M., and Dindar, M., 2001, "Turbine Blade Probabilistic Analysis Using Semi-Analytical Sensitivities", AIAA Paper No. 2001-1613, *Proceedings of the 42nd AIAA/ASME/ASCE/AHS/ASC Structures, Structural Dynamics, and Materials Conference and Exhibit*, Seattle, WA

4. Sidwell, V. and Darmofal, D., 2003, "Probabilistic Analysis of a Turbine Cooling Air Supply System: The Effect on Airfoil Oxidation Life", ASME Paper No. GT2003-38119, *Proceedings of the ASME Turbo Expo 2003: Power for Land, Sea, and Air*, Atlanta, GA

5. Moeckel, C.W., Darmofal, D.L., Kingston, T.R., and Norton, R.J.G., 2007, "Toleranced Designs of Cooled Turbine Blades Through Probabilistic Thermal Analysis of Manufacturing Variability", ASME Paper No. GT2007-28009, *Proceedings of the ASME Turbo Expo 2007: Power for Land, Sea, and Air,* Montreal, Canada

6. Jolliffe, I.T., 2002, *Principal Component Analysis*, 2nd ed., Springer, New York, pp.6-9

7. Flurry, B., 1988, *Common Principal Components and Related Multivariate Models*, John Wiley & Sons, New York, Section 2.3

8. Gnanadesikan, R., 1977, *Methods for Statistical Data Analysis of Multivariate Observations*, John Wiley & Sons, New York, pp. 7-15

9. Morrison, D.F., 1976, *Multivariate Statistical Methods*, 2nd ed., McGraw-Hill Book Company, New York, Chapter 8

10. Lay, D.C., 2006, *Linear Algebra and Its Applications*, 3rd ed., Pearson Education, Boston, Section 7.5

11. Shores, T.S., 2007, *Applied Linear Algebra and Matrix Analysis*, Springer, New York, Chapter 5

12. Garzon, V.E., 2003, "Probabilistic Aerothermal Design of Compressor Airfoils", Ph.D. Thesis, Massachusetts Institute of Technology

13. Lamb, C.M., 2005, "Probabilistic Performance-Based Geometric Tolerancing of Compressor Blades", M.S. Thesis, Massachusetts Institute of Technology

14. Hall, E.J., Heidegger, N.J., and Delaney, R.A., 1999, "ADPAC v1.0 User's Manual", NASA CR-1999-206600

15. Drela, M. and Youngren, H., 2008, "A User's Guide to MISES 2.63", MIT Aerospace Computational Design Laboratory

16. Roberts, W.B., Armin, A., Kassaseya, G., Suder, K.L., Thorp, S.A., and Strazisar, A.J., 2002, "The Effect of Variable Chord Length on Transonic Axial Rotor Performance", *ASME Journal of Turbomachinery*, Vol. 124, pp. 351-357

17. Datta, B.N., 1995, *Numerical Linear Algebra and Applications*, Brooks/Cole Publishing Company, Pacific Grove, CA, Chapter 10

18. The Mathworks, 2007, *MATLAB 7 Function Reference: Volume 3 (P-Z)*, The Mathworks, Inc., Natick, MA, pp. 2-3339-2-3341

19. Drela, M., 1998, "MISES Implementation of Modified Abu-Ghannam/Shaw Criterion", MIT Aerospace Computational Design Laboratory